Phylogenetic relationships of corytophanid lizards (Iguania, Squamata, Reptilia) based on partitioned and total evidence analyses of sperm morphology, gross morphology, and DNA data

Gustavo H. C. Vieira, Guarino R. Colli & Sônia N. Báo

Vieira, G. H. C., Colli, G. R. & Báo, S. N. (2005). Phylogenetic relationships of corytophanid lizards (Iguania, Squamata, Reptilia) based on partitioned and total evidence analyses of sperm morphology, gross morphology, and DNA data. — *Zoologica Scripta*, *34*, 605–625.
We conducted partitioned and combined Bayesian and parsimony phylogenetic analyses of corytophanid lizards (Iguania) using mtDNA, gross morphology, and sperm ultrastructure data sets. Bayesian and parsimony hypotheses showed little disagreement. The combined analysis, but not any of the partitioned ones, showed strong support for the monophyly of Corytophanidae and its three genera, *Basiliscus*, *Corytophanes*, and *Laemanctus*. *Basiliscus* is the sister taxon of a well-supported clade formed by *Corytophanes* and *Laemanctus*. The relationships of species within *Basiliscus* and *Corytophanes* received weak support, regardless of the method used. We defend those relationships as feasible and open to further testing. Data derived from the ultrastructure of spermatozoa are potentially a good source of characters for systematic inferences of Iguania and its major lineages. A Brooks Parsimony Analysis based on the geographic distributions of corytophanids and the phylogenetic tree obtained from the combined analysis suggested a Central American origin of the group, a recent colonization of northern South America, and the role of epeirogenic uplifts and the formation of lowlands during the late Tertiary in the differentiation of corytophanids.

Gustavo H. C. Vieira, Pós-graduação em Biologia Animal, Instituto de Ciências Biológicas, Universidade de Brasília, Brasília/DF, Brazil. E-mail: ghcv@unb.br

Guarino R. Colli, Departamento de Zoologia, Instituto de Ciências Biológicas, Universidade de Brasília, Brasília/DF, Brazil. E-mail: grcolli@unb.br

Sônia N. Báo, Departamento de Biologia Celular, Instituto de Ciências Biológicas, Universidade de Brasília, Brasília/DF, Brazil. E-mail: snbao@unb.br

Introduction

Iguania is a large, cosmopolitan group comprising approximately 1442 species (Uetz *et al*. 1995). Iguanians are sit-and-wait foragers that rely primarily on visual cues to locate food. Despite their typical appearance, they are diverse in form, behaviour, and ecological aspects. The monophyly of Iguania is well established (Frost & Etheridge 1989; Lee 1998; Schulte *et al*. 2003) and different authors recognize three (Macey *et al*. 1997; Schulte *et al*. 1998, 2003) or 14 (Frost *et al*. 2001) main monophyletic clades. Traditionally, three families are recognized (Camp 1923): Agamidae, Chamaeleonidae and Iguanidae, the first two being closest relatives.

Ambiguously placed within Iguania, the Neotropical family Corytophanidae (*sensu* Frost & Etheridge 1989) comprises three genera and nine species. The genus *Basiliscus*

contains four species (*B. basiliscus*, *B. galeritus*, *B. plumifrons* and *B. vittatus*) and the genera *Corytophanes* and *Laemanctus* contain three and two species, respectively (*C. cristatus*, *C. hernandesii* and *C. percarinatus*; *L. longipes* and *L. serratus*). Corytophanids range from north-western Mexico to northern South America (Colombia, Ecuador and Venezuela: Lang 1989; Uetz *et al*. 1995; Zug *et al*. 2001). They are moderate to large bodied lizards that inhabit dry scrub forest and wet rainforest. Two of the most ecologically distinct characteristics of *Basiliscus* are the capability to run bipedally and across the water surface, sometimes seeking refuge underwater. *Corytophanes* and *Laemanctus* are strongly arboreal, whereas *Basiliscus* is most frequently encountered on the ground (low-level microhabitats), seeking refuges and basking perches on trees and shrubs (Zug *et al*. 2001). Corytophanids

are evidently distinct from other iguanians by the presence of an extended parietal crest (Frost & Etheridge 1989; Lang 1989), sexually dimorphic in *Basiliscus* (Lang 1989; Pough *et al*. 1998). In summary, they can be described as crest- or casque-headed, long-limbed, long-tailed and slender-bodied (Zug *et al*. 2001). A good review of the distribution, natural history and taxonomy of corytophanid lizards was provided by Lang (1989).

Previously known as Basiliscinae (basiliscines) (Etheridge & de Queiroz 1988; Lang 1989), the taxonomic status of Corytophanidae has changed over the decades. The group was recognized as a family (along with seven more iguanid *sensu lato* lineages) by Frost & Etheridge (1989) but the taxonomy of Iguania is a quodlibet (see Schwenk 1994; Macey *et al*. 1997; Schulte *et al*. 1998, 2003; Frost *et al*. 2001). Several studies attempted to establish the phylogenetic position of iguanian clades using molecular, morphological (Etheridge & de Queiroz 1988; Frost & Etheridge 1989; Lang 1989) and combined data sets (Macey *et al*. 1997; Schulte *et al*. 1998, 2003; Frost *et al*. 2001), but all led to the same conclusion: the available data are unable to recover a well-supported grouping for those lineages. Thus, the sister group of Corytophanidae is still unknown. Some authors proposed relationships of corytophanids with polychrotids (Frost & Etheridge 1989; Frost *et al*. 2001) and acrodonts (Frost & Etheridge 1989), but these relationships were either not well supported (Frost & Etheridge 1989) or could not be accepted with conviction (see Schulte *et al*. 2003). Regardless of its sister group, however, the monophyly of Corytophanidae is not contested (Frost & Etheridge 1989; Lang 1989; Schulte *et al*. 2003). We here adopt the taxonomic accounts by Frost & Etheridge (1989) and Frost *et al*. (2001) in which all groups of Iguanidae (*sensu lato*) were raised to family status and Iguanidae (*sensu lato*) was synonymized with Pleurodonta.

A phylogeny of Corytophanidae was first proposed by Etheridge & de Queiroz (1988) and later corroborated by Lang (1989) and Frost & Etheridge (1989). All those works used morphological data and concluded that *Basiliscus* is the sister group of *Corytophanes* plus *Laemanctus*. However, Schulte *et al*. (2003), using molecular and morphological data, presented some cladograms in which *Basiliscus* is the sister group of *Laemanctus* (their figures 1 and 5) or some in which the support for the grouping of *Corytophanes* plus *Laemanctus* is weak (their figures 2, 3 and 4). They provided few explanations for this, focusing their discussion on the support for major iguanian lineages and their taxonomy.

Since Etheridge & de Queiroz (1988), Lang (1989) and Frost & Etheridge (1989), methods employed for phylogenetic inference have changed drastically. Not surprisingly, some advances have also occurred in the discovery of new data sets. Molecular data are widely used and need no comment. Sperm ultrastructure has received considerable atten-

tion for reptile (mainly squamate) groups (Jamieson 1995b; Jamieson *et al*. 1996; Teixeira *et al*. 1999b,c; Giugliano *et al*. 2002; Tavares-Bastos *et al*. 2002; Teixeira 2003; Vieira *et al*. 2004). The growing characterization of the sperm cell among iguanian lizards (Teixeira *et al*. 1999a,d; Scheltinga *et al*. 2000, 2001; Vieira *et al*. 2004) could help to resolve the phylogenetic relationships among and within major iguanian lineages. We here use the ultrastructure of the spermatozoon, 'gross morphology' (provided by Frost & Etheridge 1989; Lang 1989) and molecular characters to conduct Bayesian and parsimony phylogenetic analyses of Corytophanidae.

Materials and methods

Data sets and taxa

We used three data sets in phylogenetic analyses: molecular, gross morphology (hereafter simply called morphological data) and sperm ultrastructure. Unfortunately, not all taxa could be sampled for all data sets. Therefore, we used more exclusive taxonomic ranks to assign character-states to some taxa. This approximation, however, was done only for outgroup taxa. We used members of Scleroglossa, Iguanidae, Polychrotidae and Tropiduridae as representative outgroup taxa (Table 1). We used all nine corytophanid species in the combined analysis.

Molecular data were derived from Schulte *et al*. (2003). Their data comprise partial mitochondrial DNA sequences that include 1838 aligned positions extending from the protein-coding gene *ND1* (subunit I of NADH dehydrogenase) through the genes encoding tRNA[Ile], tRNA[Gln], tRNA[Met], protein-coding gene *ND2* (subunit II of NADH dehydrogenase), tRNA[Trp], tRNA[Ala], tRNA[Asn], tRNA[Cys], tRNA[Tyr], to the protein-coding gene *COI* (subunit I of cytochrome c oxidase). tRNA genes were aligned by using secondary structural models, whereas protein encoding genes (*ND1*, *ND2* and *COI*) were aligned by eye and translated to amino acids for further confirmation of the alignment (for details see Schulte

Table 1 Outgroup taxa used as representatives of each data set.

Data type	Taxon name	Source
Molecular	*Elgaria panamintina* (Anguidae)	Schulte *et al*. 2003
	Sauromalus obesus (Iguanidae)	
	Polychrus acutirostris (Polychrotidae)	
	Tropidurus etheridgei (Tropiduridae)	
Morphological	Scleroglossa	Frost & Etheridge 1989/
	Iguanines (Iguanidae)	Lang 1989
	Polychrus/anoloids (Polychrotidae)	
	Tropidurus/tropidurines (Tropiduridae)	
Sperm	*Teius oculatus* (Teiidae)	Teixeira 2003
	Iguana iguana (Iguanidae)	Vieira *et al*. 2004
	Polychrus acutirostris (Polychrotidae)	Teixeira *et al*. 1999a
	Tropidurus torquatus (Tropiduridae)	Teixeira *et al*. 1999d

et al. 2003). We downloaded their data matrix from Tree-BASE (http://www.treebase.org/treebase/index.html; study accession S847; matrix accession number M1365), excluding questionable and unalignable regions (218 positions) from our analyses. This left only one region (three base positions long, from position 1288 to 1290) with gaps and we implemented the 'simple indel coding' method of Simmons & Ochoterena (2000) to include this region in our analyses. For the ingroup, we used mtDNA data for *Basiliscus galeritus*, *B. plumifrons*, *B. vittatus*, *Corytophanes cristatus*, *C. percarinatus* and *Laemanctus longipes*. Molecular characters ranged from characters 1 through 1838 (see data matrix on the TreeBASE website: study accession number = S1329; Matrix accession number M2333).

We obtained morphological characters from Lang (1989) and Frost & Etheridge (1989). We excluded some of their original characters to avoid any character being represented twice in our matrix (see Appendix 1). Morphological characters ranged from character 1872 to 1960 (89 characters; TreeBASE Matrix accession number = M2332).

Epididymal tissues from two specimens of *Basiliscus vittatus*, *Corytophanes cristatus* and *Laemanctus longipes* were kindly supplied by Dr James C. O'Reilly (University of Miami). We used traditional electron-microscopy methods to evaluate character states derived from sperm ultrastructure (see Vieira *et al.* 2004). Voucher specimens were deposited in Coleção Herpetológica da Universidade de Brasília (CHUNB 29712–29716 and 29660). Sperm characters are of two types: discrete and morphometric (quantitative). Additionally, in this work we recorded morphometric characters for the sperm of *Polychrus acutirostris* and *Tropidurus torquatus*. Sperm derived characters ranged from character 1840 to 1871 (32 characters; TreeBASE Matrix accession number = M2331). Character names for morphological and sperm-derived data sets are listed in Appendix 1.

Phylogenetic analyses

Morphometric data were treated as continuous quantitative variables and coded using the step matrix gap-weighting method of Wiens (2001). Step matrices for each morphometric character are provided in the data matrix (TreeBASE website). Fixed multistate characters were ordered according to the morphological intermediacy method proposed by Wilkinson (1992). Character name and states and ordered characters are shown in Appendix 1.

We used the equal-weighted parsimony method for maximization of congruence over all data (Grant & Kluge 2003). Parsimony analyses were conducted on the combined data set (TreeBASE Matrix accession number = M2330) and on each partition (molecular, morphological and sperm-derived). We conducted branch-and-bound searches for morphological and combined analyses. All other analyses (molecular and sperm

only) were conducted through exhaustive searches. All analyses were constrained to ensure the monophyly of Iguania. All discrete characters were weighted 999 and all quantitative morphometric characters received weight 1 (in sperm-derived partitioned analysis and combined analysis; Wiens 2001). Consequently, all analyses that use this weighting scheme produce cladograms with lengths (and branch support) multiplied by 999. Therefore, we divided the length of those cladograms by 999, allowing comparisons with other studies (hereafter the raw length of those cladograms is shown in parentheses).

Branch support (Bremer 1994) was used to evaluate clade support, calculated via default heuristic search as implemented in MacClade (Maddison & Maddison 2001). Felsenstein (1985) concluded that a minimum of four characters (even with data showing both perfect compatibility and no character conflict) must support the choice of a significantly accepted tree. Since branch support is the number of extra steps required before a clade is lost from the most parsimonious cladogram (or strict consensus tree), Macey *et al.* (1997) used branch support with a cut-off value of 4 to indicate strongly supported groups, based on Felsenstein's (1985) conclusion. We think this approach is reasonable and use it in this study. We divided the raw branch support index by 999 for sperm-derived partitioned and combined analyses (for the same reason outlined above). We used MacClade (Maddison & Maddison 2001) and PAUP* (Swofford 2002) for all data management and parsimony analyses.

Bayesian analyses were conducted with MrBayes (Huelsenbeck & Ronquist 2001) using two main partitions: one for molecular and the other for morphological data. Schulte *et al.* (2003) used Modeltest (Posada & Crandall 1998) to evaluate 56 models of sequence evolution in order to identify the one that best fits the data, by using hierarchical ratio tests; all those models are implemented in MrBayes (J. A. Schulte, pers. comm.). They demonstrated that the GTR + I + Γ model best explains the DNA sequence data. The parameters of the model were estimated from the sequence data in each analysis in MrBayes, with the vertebrate mitochondrial genetic code enforced (because this code is slightly different from the universal genetic code, particularly in reference to methionine and stop codons). Additionally, the priors on DNA state frequencies were empirically estimated from the data. All other parameters and priors of the phylogenetic model were the default ones of MrBayes.

We used the gamma-distributed rates model for among-site rate variation across sites (characters), using the symmetrical beta distribution (with the five default rate categories) to model the stationary frequencies for morphological characters. Those parameters approximate a well-behaved Markov model (mainly by making the likelihood conditional on characters being variable, since constant characters are absent

in morphological data sets) for estimating morphological phylogenies using the likelihood criterion (Lewis 2001). All other parameters and priors of the phylogenetic model for morphological characters were the default of MrBayes. We extended the character ordering implemented in parsimony analyses in Bayesian phylogenetic analyses.

Continuous morphometric characters were excluded from Bayesian analyses because MrBayes cannot apply weights and step matrices. All Bayesian analyses were started from random trees and were run for 2 000 000 generations. Trees were sampled every 100 generations, resulting in 20 000 sampling points (trees). We plotted the log-likelihood scores of the 20 000 trees against generation time to detect when stationarity was attained. All sample points before stationarity were considered burn-in samples that contained no useful information about parameters. Stationarity was obtained after the 5000th generation. Stationarity indicates convergence of log-likelihood values and all trees produced after that can be used to produce a 50% majority-rule consensus tree in PAUP*, with the percentage of trees recovering a particular clade denoting the clade's posterior probability (Huelsenbeck & Ronquist 2001). In this way, we used 45 000 trees (the remaining 15 000 [20 000 minus 5000 burn-in trees] of each independent run times three runs; see below) to compute the posterior probability of the clades. We used percentage values ≥ 95% as indicating a significantly supported clade.

Finally, we avoided trapping on local optima by running three independent analyses, beginning with different starting trees and analysing their log-likelihood values for convergence and by evaluating convergence of the posterior probabilities for individual clades. In addition, the variant of Markov Chain Monte Carlo implemented in MrBayes, the Metropolis-coupled Markov Chain Monte Carlo (MCMCMC or MC3), readily explores the space of phylogenetic trees through heated chains by lowering optimal peaks and filling in valleys. Thus, the cold chains can better jump across deep valleys in the landscape of trees, avoiding trapping on local optima (Huelsenbeck & Ronquist 2001). We used four incrementally heated Markov chains (program default) to amplify their tree-climbing quality.

Brooks parsimony analysis

We used Brooks Parsimony Analysis (BPA, Brooks 2001) to investigate the historical biogeography of corytophanids. We obtained geographical distributions from Townsend *et al*. (2004a,b) for *C. cristatus* and *C. percarinatus*, from McCranie *et al*. (2004) for *C. hernandesii*, from McCranie & Köhler (2004a,b) for *Laemanctus* and from Lang (1989) for *Basiliscus*. To conduct BPA, we divided the geographical range of corytophanids into six regions based on species distributions, altitude and putative geographical barriers. These are, from north to south: (1) central Mexico, from Jalisco and Tamaulipas to the Isthmus of Tehuantepec; (2) the Yucatan peninsula; (3) the northern Atlantic lowlands, from Gracias a Dios in eastern Honduras to San Juan del Norte in south-eastern Nicaragua; (4) central highlands, from Chiapas to the Cordillera Chontaleña, in southern Nicaragua; (5) Costa Rica-western Panama, from the Cordillera de Guanacaste to the Isthmus of Panama; and (6) eastern Panama-northern South America, from the Isthmus of Panama to Guayaquil, Ecuador. Using these regions as taxa and presence/absence of corytophanid species and their ancestors as characters, we built a matrix that was subjected to parsimony analysis using PAUP* v. 4.0b10, with all characters ordered (TreeBASE Matrix accession number = M2329). We rooted the resulting tree using an all-zero outgroup.

Results

Sperm morphology

The spermatozoa of *Basiliscus vittatus*, *Corytophanes cristatus* and *Laemanctus longipes* are all similar in structure. They are filiform, consisting of a head region (nucleus and acrosome cap), midpiece (containing the mitochondria) and tail (the flagellar region). The whole sperm of *B. vittatus* is represented diagrammatically in Fig. 1, while Fig. 2I shows the sperm under Nomarski light microscopy. Morphometric characters are summarized in Table 2.

Acrosome complex and nucleus

The acrosome complex is curved apically (Fig. 2A,I,K). Its most anterior portion has a spatulate aspect (Fig. 2K). It consists of two conical caps, the external acrosome vesicle and the internal subacrosomal cone (Fig. 2A,D–G). The acrosome vesicle is divided into two portions (Fig. 2B,C,J): the internal, moderately electron-dense medulla and the external, more electron-dense and thinner cortex. Posteriorly, the acrosome vesicle is more homogeneous and presents a unilateral ridge (Fig. 2D,E). More anteriorly, the ridge becomes bilateral (Fig. 2F) and finally disappears at the posterior end of the acrosome complex (Fig. 2G). Within the medulla, the perforatorium is an elongate, inclined and narrow rod with a pointed tip (Fig. 2A). The subacrosomal cone covers the anterior portion of the nucleus, the nuclear rostrum (Fig. 2A); it appears paracrystalline and homogeneous in longitudinal section (Fig. 2A,J). A fragmented epinuclear electron-lucent zone is present at the anterior portion of the nuclear rostrum (Fig. 2J).

The nucleus is cylindrical, elongate and slightly curved. It consists of a homogeneous, electron-dense and highly compacted chromatin (Fig. 2A,H). Nuclear lacunae are frequently observed (Fig. 2H). The nuclear rostrum is cone-shaped and invades a substantial portion of the subacrosomal cone, from the subacrosomal flange to the epinuclear electron-lucent zone (Fig. 2A,E–G). The posterior region of the
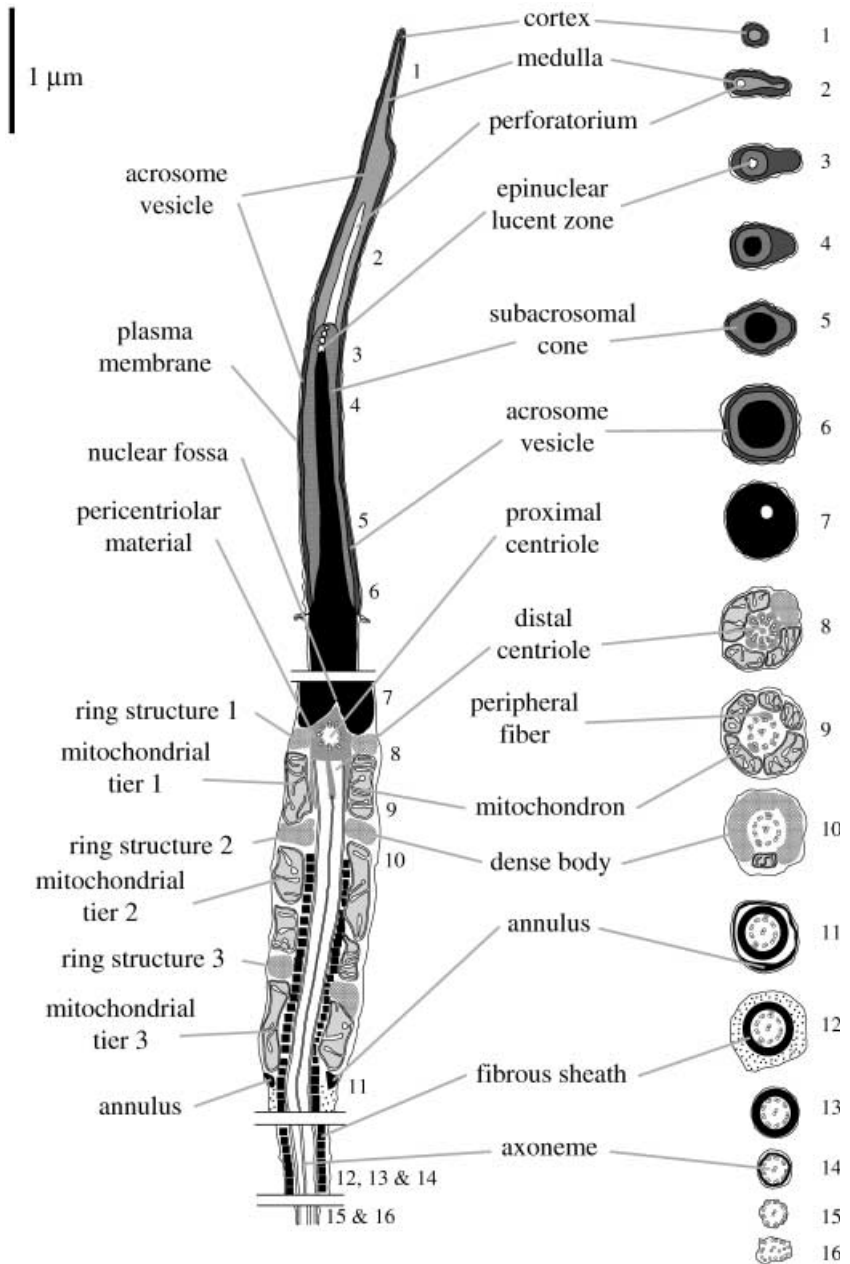
Fig. 1 Schematic drawing of mature spermatozoon of *Basiliscus vittatus* in longitudinal section and each corresponding transverse section. The numbers next to each transverse section indicate the corresponding region in the longitudinal section. All structures are proportionally drawn. Drawn from TEM micrographs.

nucleus, the nuclear fossa, is shaped like a narrow conical hollow within which the neck elements reside (Fig. 3A,J,K).

Neck region and midpiece

The neck region connects the head to the midpiece and tail. It has two centrioles, the first ring of dense bodies and the pericentriolar material (Fig. 3A,K). The proximal centriole is closely fitted and centrally located at the nuclear fossa (Fig. 3A,K). In *C. cristatus* and *L. longipes* it has a rounded, centrally located, electron-dense structure in its interior

(Fig. 3A). This structure is absent in *B. vittatus* (Fig. 3K). Immediately posterior (and with perpendicular orientation) to the proximal centriole, the distal centriole represents the basal body of the axoneme and is the first axial component of the midpiece (Fig. 3A,K). The distal centriole extends into the midpiece (Fig. 3A,K). It consists of nine triplets of microtubules, nine peripheral fibres that partially cover the triplets and the two central singlets of the axoneme (Fig. 3B). Both centrioles are encircled by homogeneously electron-dense material (the pericentriolar material) that matches the shape

Table 2 Mean, standard deviation and number of observations of each morphometric character for sperm of outgroup and ingroup taxa. All measurements in micrometers, except the percentage of fibrous sheath occupancy within the midpiece (FSOM). The mean of particular morphometric characters was used to code states, according to the step matrix gap-weighting method of Wiens (2001).

Character	T. oculatus	I. iguana	P. acutirostris	T. torquatus	B. vittatus	C. cristatus	L. longipes
AL	2.88 ± 0.23 (10)	4.88 ± 0.35 (15)	4.30 ± 0.58 (11)	4.01 ± 0.22 (11)	4.35 ± 0.35 (16)	4.41 ± 0.30 (11)	4.58 ± 0.38 (12)
DCL	0.86 ± 0.09 (10)	1.23 ± 0.27 (12)	0.73 ± 0.17 (19)	0.74 ± 0.10 (13)	0.73 ± 0.06 (11)	0.66 ± 0.05 (15)	0.73 ± 0.09 (13)
ETL	0.11 ± 0.04 (6)	0.48 ± 0.08 (16)	0.29 ± 0.05 (10)	0.51 ± 0.06 (15)	0.32 ± 0.09 (10)	0.46 ± 0.09 (10)	0.26 ± 0.05 (10)
ETW	0.05 ± 0.00 (6)	0.08 ± 0.02 (16)	0.06 ± 0.01 (10)	0.07 ± 0.02 (15)	0.10 ± 0.04 (10)	0.09 ± 0.02 (10)	0.08 ± 0.02 (10)
FSOM	0.85 ± 0.01 (10)	0.57 ± 0.04 (10)	0.77 ± 0.02 (11)	0.62 ± 0.05 (13)	0.66 ± 0.02 (13)	0.71 ± 0.04 (14)	0.66 ± 0.02 (10)
HL	18.91 ± 2.50 (11)	18.22 ± 1.39 (12)	17.15 ± 0.70 (11)	19.53 ± 0.85 (12)	18.31 ± 0.42 (14)	18.43 ± 0.63 (18)	18.37 ± 1.01 (20)
MPL	3.54 ± 0.36 (11)	3.36 ± 0.38 (16)	3.84 ± 0.44 (13)	2.63 ± 0.27 (19)	2.91 ± 0.22 (15)	3.02 ± 0.22 (15)	3.02 ± 0.21 (11)
NBW	0.46 ± 0.05 (10)	0.53 ± 0.04 (14)	0.58 ± 0.07 (16)	0.55 ± 0.06 (13)	0.56 ± 0.06 (14)	0.57 ± 0.06 (11)	0.54 ± 0.04 (14)
NL	16.04 ± 2.50 (11)	13.34 ± 1.39 (12)	12.85 ± 0.70 (11)	15.52 ± 0.85 (12)	14.19 ± 0.42 (14)	14.22 ± 0.63 (18)	13.66 ± 1.01 (20)
NRL	0.66 ± 0.04 (6)	2.62 ± 0.25 (10)	2.33 ± 0.21 (11)	1.70 ± 0.14 (15)	2.31 ± 0.19 (13)	2.40 ± 0.18 (11)	2.77 ± 0.34 (10)
NSW	0.34 ± 0.03 (10)	0.34 ± 0.06 (10)	0.37 ± 0.04 (15)	0.37 ± 0.05 (10)	0.48 ± 0.08 (16)	0.43 ± 0.05 (10)	0.43 ± 0.02 (8)
TaL	53.20 ± 6.96 (10)	49.50 ± 5.54 (12)	62.94 ± 2.74 (11)	70.67 ± 3.91 (12)	68.17 ± 1.73 (14)	73.59 ± 1.97 (18)	75.70 ± 1.51 (20)
TL	74.74 ± 10.73 (10)	71.69 ± 2.43 (12)	83.70 ± 3.07 (11)	93.17 ± 2.44 (12)	90.31 ± 1.53 (14)	96.11 ± 2.50 (18)	97.65 ± 2.27 (20)

Abbreviations: acrosome complex length (AL), distal centriole length (DCL), epinuclear lucent zone length (ETL), epinuclear lucent zone width (ETW), percentage of fibrous sheath occupancy within the midpiece (FSOM), head length (HL), midpiece length (MPL), nuclear base width (NBW), nuclear length (NL), nuclear rostrum length (NRL), nuclear shoulders width (NSW), tail length (TaL), total length (TL).

of the deep nuclear fossa and is connected with the anterior portion of the distal centriole, like the dense peripheral fibres (Fig. 3A,K). A discrete laminar structure projects bilaterally from the pericentriolar material (Fig. 3K).

The midpiece begins at the nuclear fossa, incorporating the neck elements and terminates at the most posterior electron-dense ring, the annulus (Fig. 3A). The midpiece consists of the neck and flagellar components surrounded by mitochondrial gyres and dense body rings. The beginning of the fibrous sheath marks the transition between the distal centriole and the axoneme (Fig. 3A,K). The axoneme is characteristically arranged in a 9 + 2 pattern of double microtubules surrounded by the fibrous sheath (Fig. 3C,D). The peripheral dense fibres extend from the pericentriolar material and decrease in size with the exception of fibres 3 and 8, which are grossly enlarged through the anterior portion of the midpiece (Fig. 3C). The fibrous sheath encircles the axoneme, forming a complete and electron-

dense ring in transverse section (Fig. 3C–E). It comprises regularly spaced, dense, square blocks (Fig. 3A).

Mitochondria are sinuous tubules (Fig. 3J) that form regular tiers in sections that have a perfect longitudinal orientation (Fig. 3A). They surround the distal centriole and axoneme and have linear cristae (Fig. 3A). In transverse section, they appear trapezoidal, usually forming from 5 to 6 elements around the axoneme (Fig. 3D). Dense bodies are complete or interrupted rings (ring structures) interposed among mitochondrial tiers (Fig. 3A–C). There are three irregularly spaced rings, the first in the vicinity of the proximal centriole, in the neck region (Fig. 3A,J,K). The rings are formed by granular structures, not delimited by membranes and lie juxtaposed to the fibrous sheath. Associated with each dense body ring there is a posterior ring of mitochondria, which gives the midpiece an aspect of three identical sets of mitochondria/dense bodies, represented as rs1/m1, rs2/m2

Fig. 2 A–K. Head region of mature spermatozoon of corytophanid lizards. A–H; J–K: transmission electron micrographs; I: Nomarski light micrograph. —A. Longitudinal section (LS) through the anterior portion of the nucleus and through the acrosome complex, showing the nuclear rostrum, the subacrosomal cone, the acrosome vesicle, the epinuclear electron-lucent, 38 500×. —B–G. Corresponding transverse sections of the acrosome complex. Note that the acrosome complex becomes highly depressed, from its base (G) to its apex (B). —B. Most anterior portion of the acrosome complex, 55 000×. —C. Acrosome vesicle at the perforatorium level showing its subdivision into cortex and medulla, 55 555×. —D. Transverse section (TS) through the epinuclear electron-lucent zone; note that the acrosome complex is unilaterally ridged, 47 407×. —E–F. TS through the nuclear rostrum; the acrosome complex is still unilaterally ridged most anteriorly, but shifts to bilaterally shaped most posteriorly, 47 407× and 55 000× respectively. —G. TS of the most posterior portion of the acrosome complex, 56 000×. —H. TS of the nucleus, showing a lacuna, 58 261×. —I. Nomarski light micrograph of the entire sperm cell, 6615×. —J. LS through the acrosome complex showing the fragmented electron-lucent zone, highly electron-dense cortex and moderate electron-dense medulla, 47 060×. —K. LS of the acrosome complex showing the funnel shape of the acrosome vesicle, 25 000×. *Abbreviations*: av: acrosome vesicle; c: cortex of the acrosome vesicle; et: epinuclear electron-lucent zone; h: head; me: medulla of the acrosome vesicle; mp: midpiece; n: nucleus; nr: nuclear rostrum; p: perforatorium; pm: plasma membrane; sc: subacrosomal cone; t: tail; ur: unilateral ridge. A, C, D, E, G and J from *B. vittatus*; H from *C. cristatus*; B, F, I and K from *L. longipes*.
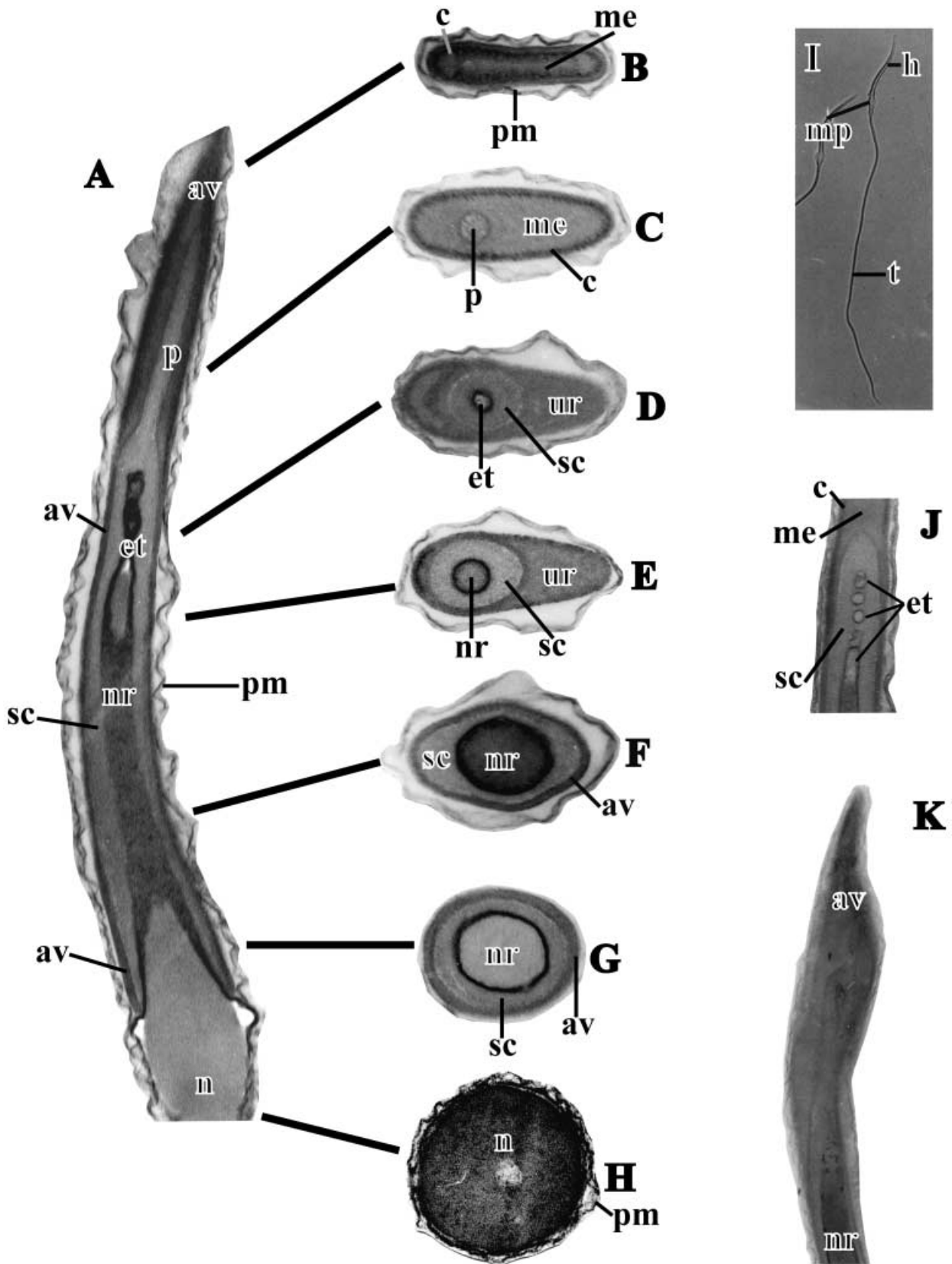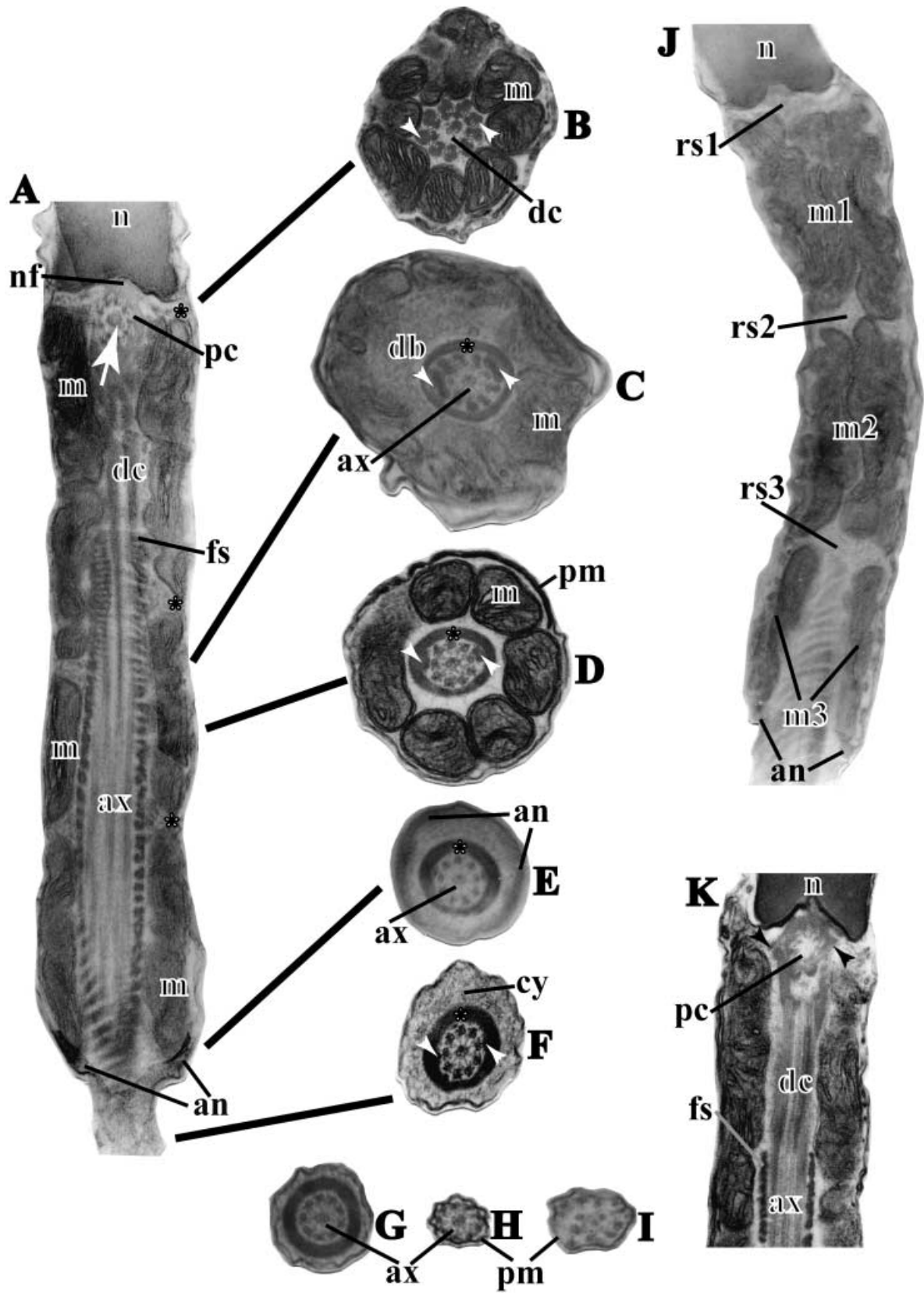
and rs3/m3 (Fig. 3J). In transverse section, dense bodies can form irregular and complete rings or incomplete rings interrupted by mitochondria (Fig. 3C). Finally, the midpiece ends at a small dense ring, the annulus, with triangular aspect in longitudinal section and irregular aspect in transverse section (Fig. 3A,E,J).

Principal piece and endpiece

The principal piece starts posteriorly to the annulus and is composed of the plasma membrane encircling the fibrous sheath and the axoneme (Fig. 3F,G). The principal piece and endpiece form the sperm tail. In its anterior region, a large mass of finely granular cytoplasm is observed between the membrane and the fibrous sheath (Fig. 3F), which decreases the diameter of the transition between the midpiece and the principal piece. Within this transition, fibres 3 and 8 are still present (Fig. 3F). Posteriorly, the principal piece is solely composed of the plasma membrane juxtaposed to the fibrous sheath, with fibres 3 and 8 absent (Fig. 3G).

The endpiece is characteristically marked by the absence of the fibrous sheath. This region of the tail has a reduced diameter, with its anterior portion maintaining the 9 + 2 axonemal microtubule arrangement (Fig. 3H) and the posterior portion with disordered microtubules, the doublets being separated (Fig. 3I).

Parsimony analyses

We conducted four different parsimony analyses: one on each data partition (molecular, morphological and sperm-derived data) and one on the combined data. The analysis of the molecular partition produced one most parsimonious cladogram of 1787 steps, consistency index (CI) of 0.654 and retention index (RI) of 0.382 (Fig. 4A). Molecular data (1621 characters, 488 parsimony-informative) recovered a monophyletic Corytophanidae (branch support of 25), *Basiliscus* (5) and *Corytophanes* (35). In addition, they recovered a clade composed of *Corytophanes* plus *Laemanctus*, but the support for this branch (3) was weak.

Morphological data produced four equally most parsimonious cladograms (89 characters, 70 parsimony-informative), 147 steps long (CI = 0.7415, RI = 0.8288). The strict consensus tree (Sokal & Rohlf 1981) of those cladograms is depicted in Fig. 4B. It shows *P. acutirostris* as the sister taxon of *Corytophanes* plus *Laemanctus*, but this group received very low branch support. The morphological partition supported a monophyletic *Basiliscus* (branch support of 5), *Corytophanes* (14) and *Laemanctus* (6). Furthermore, the grouping of *Corytophanes* plus *Laemanctus* was also well supported (branch support of 8).

Sperm-derived data (32 characters, 25 parsimony-informative) produced a single cladogram, with 45.349 (45 394) steps, (CI = 0.749, RI = 0.590). It retrieved only Corytophanidae as strongly supported (branch support of 4) monophyletic group (Fig. 4C). It grouped *Basiliscus* with *Corytophanes*, but this group received weak support (Fig. 4C).

Combined analysis (1742 characters, 583 parsimony-informative) produced a single cladogram of 1986.337 (1 984 351) steps, (CI = 0.660, RI = 0.460). The following groups received strong support (Fig. 4D): Corytophanidae (branch support of 42), *Corytophanes* plus *Laemanctus* (8), *Basiliscus* (11), *Corytophanes* (16) and *Laemanctus* (6). Moreover, any other grouping received weak branch support, such as the relationships of Corytophanidae with other iguanids and relationships within *Basiliscus* or *Corytophanes* (Fig. 4D). The apomorphy list for each ingroup member is shown in Appendix 2.

Bayesian analyses

We conducted four Bayesian phylogenetic analyses: one for each partition and one for the combined partitions (without morphometric data). Results differed slightly from parsimony analyses. Molecular data produced a 50% majority-rule consensus tree with mean log-likelihood of −29 115.87 and variance of 15.47. It differed from parsimony molecular-only analysis in that Scleroglossa, *Tropidurus* and a well-supported clade (percentage values of 98%) formed by Iguanidae +

Fig. 3 A–K. Midpiece and tail region of mature spermatozoon of corytophanid lizards (transmission electron micrographs). —A. Longitudinal section (LS) through the midpiece showing the arrangements of mitochondria and dense bodies. Note the rs1/m1, rs2/m2, rs3/m3 arrangement of mitochondria and dense bodies. Asterisks indicate dense bodies and arrow points to the central density inside the proximal centriole, present in *C. cristatus* and *L. longipes*, 44 094×. —B–I. Series of transverse sections of the tail. —B. Neck region showing the distal centriole. The arrowheads show the peripheral fibres, 45 454×. —C. Through a dense body ring (ring structure) surrounding the axoneme, showing fibres 3 and 8 enlarged (arrowheads). Asterisk indicates the fibrous sheath, 44 783×. —D. Through a mitochondrial ring. Asterisk as in C, 46 286×. —E. Through the annulus level. Asterisk as in C and D, 46 636×. —F. Anterior portion of the principal piece, with a large portion of cytoplasm. The arrowheads point to fibres 3 and 8 and the asterisk indicates the fibrous sheath, 36 364×. —G. Medial portion of the principal piece. The plasma membrane is closely associated to the fibrous sheath, 44 615×. —H. Anterior region of the endpiece. The axoneme remains organized, 44 000×. —I. Posterior portion of the endpiece, with no axonemal organization of microtubules, 60 000×. —J. Oblique LS of the midpiece showing the columnar mitochondria and the dense body rings, 37 876×. —K. LS of the midpiece of *B. vittatus*, showing the absence of the central density inside the proximal centriole. Arrowheads point to the discrete bilateral laminar structure, 36 364×. *Abbreviations*: an: annulus; ax: axoneme; cy: cytoplasm; db: dense body; dc: distal centriole; fs: fibrous sheath; m: mitochondrion; pc: proximal centriole; pm: plasma membrane; rs: ring structure. K from *B. vittatus*; A, E and G–J from *C. cristatus*; B–D and F from *L. longipes*.
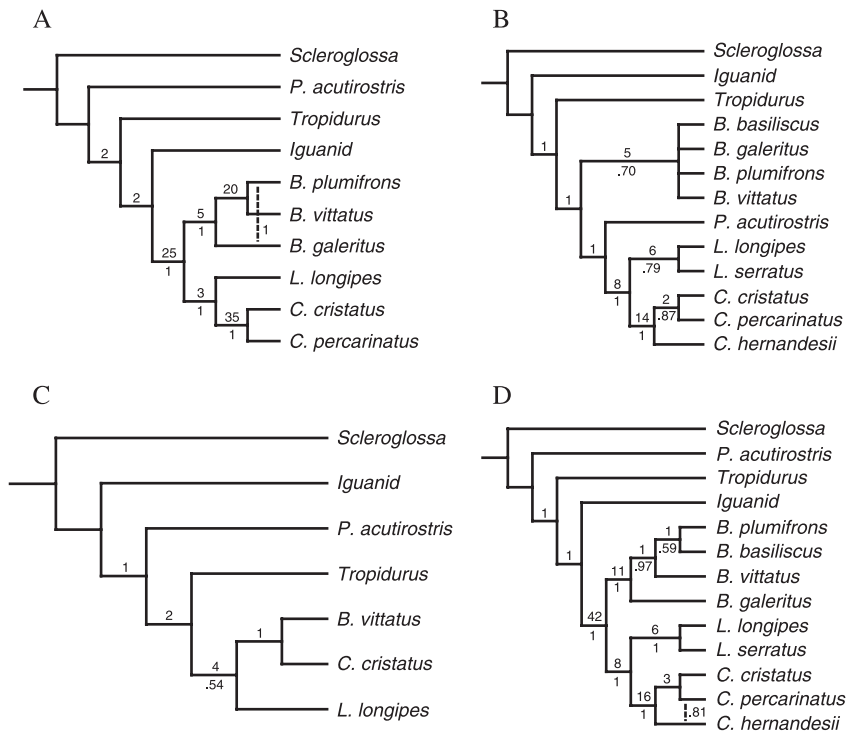
Fig. 4 A–D. Cladograms depicting the phylogenetic relationships of corytophanid lizards. —A–C. Cladograms derived from partitioned analyses. —A. Molecular data (exhaustive search); length = 1787, CI = 0.654, RI = 0.382; log likelihood = −29 115.87. —B. Morphological data (branch-and-bound search; strict consensus tree of four most parsimonious trees); all four most parsimonious cladograms with length = 147, CI = 0.741, RI = 0.829; log likelihood = −472.31. —C. Sperm derived data (exhaustive search); length = 45.349 (45 394), CI = 0.749, RI = 0.590; log likelihood = −83.50. —D. Cladogram derived from combined analysis (branch-and-bound search); length = 1986.337 (1 984 351), CI = 0.660, RI = 0.460; log likelihood = −12 162.80. Numbers above branches indicates the branch (Bremer) support and numbers below branches are Bayesian posterior probabilities. No assignment of posterior probability to a branch signifies that the clade was not recovered in Bayesian analysis and dashed lines represent alternative placement of taxa in Bayesian analysis topology (see text).

Polychrus acutirostris + Corytophanidae (82%) formed a basal polytomy. All ingroup taxa were well-supported (100%) and the only difference from parsimony analysis was that *Basiliscus vittatus*, rather than *B. galeritus*, is the first diverging taxon within *Basiliscus* (Fig. 4A).

Morphological data (gross-morphology data) produced a 50% majority-rule consensus tree with mean log-likelihood of −472.31 and variance of 13.76. It differed from the parsimony morphological tree in the placement of outgroup taxa but relationships among ingroup taxa were the same. Support for *Corytophanes* + *Laemanctus* and *Corytophanes* was achieved, but there was low support for Corytophanidae, *Basiliscus* and *Laemanctus* (Fig. 4B).

Sperm data (discrete characters only) produced a 50% majority-rule consensus tree with mean log-likelihood of −83.50 and variance of 5.54. The tree is a polytomy among all outgroup taxa and corytophanids, but with low support for the latter (Fig. 4C). This was somewhat expected, due to the elimination of the continuous morphometric characters.

Combined data analysis produced a 50% majority-rule consensus tree with mean log-likelihood of −12 162.80 and variance of 17.91. Again, the placement of outgroups differed from parsimony analysis, with *P. acutirostris* being the sister taxon of Corytophanidae (support of 64%) and Iguanidae + *Tropidurus* receiving weak support (53%) (and forming a polytomy with the previous group and Scleroglossa). Posterior probability values for Corytophanidae, *Basiliscus*, *Corytophanes*,

Laemanctus, *Corytophanes* + *Laemanctus* and (*B. vittatus* + *B. basiliscus* + *B. plumifrons*) were high (Fig. 4D). The only difference in the arrangement of ingroup taxa between Bayesian and parsimony analyses was on the placement of *C. hernandesii* relative to the other species of *Corytophanes*: in parsimony analysis, *C. hernandesii* is the sister taxon of the remaining taxa, while in Bayesian analysis it forms a poorly supported clade with *C. percarinatus* (Fig. 4D).

Brooks parsimony analysis

We used the phylogenetic tree resulting from the combined data analysis in BPA (Table 3, Fig. 5A). BPA produced a single most parsimonious area cladogram (Fig. 5B), in which there is a basal dichotomy separating a southern group of areas, comprising the northern Atlantic lowlands + Costa Rica-western Panama + eastern Panama-northern South America, from a northern bloc comprising the central highlands + central Mexico + Yucatan. The southern group was supported by the presence of *Basiliscus galeritus* and *Corytophanes cristatus*, whereas the northern bloc was supported by the ranges of *Laemanctus longipes*, *L. serratus* and their ancestor. Further, BPA suggested a closer relationship between Costa Rica-western Panama and eastern Panama-northern South America, supported by the presence of *B. basiliscus* and the ancestor of *B. basiliscus* and *B. plumifrons* and between central Mexico and Yucatan, supported by the range of *C. hernandesii*. The resulting area cladogram implied in two

Table 3 Matrix listing the six regions of Central America, the species that inhabit them (characters 1–9), the putative ancestors of the groups resulting from the combined analysis (characters 10–17) and the binary codes representing those species and their phylogenetic relationships. See Fig. 5A and text.

	1	2	3	4	5	6	7	8	9	10	11	12	13	14	15	16	17
CM	0	0	1	0	1	1	0	0	1	0	1	1	1	0	1	1	1
Y	0	0	1	0	1	1	1	0	1	0	1	1	1	1	1	1	1
NAL	0	0	1	0	0	0	1	0	0	0	1	1	0	1	1	1	1
CH	0	0	1	0	1	1	0	1	0	0	1	1	1	1	1	1	1
CRWP	1	1	1	1	0	0	1	0	0	1	1	1	0	1	1	1	1
EPNSA	0	1	1	1	0	0	1	0	0	1	1	1	0	1	1	1	1
Ancestral	0	0	0	0	0	0	0	0	0	0	0	0	0	0	0	0	0

Abbreviations: central Mexico (CM), Yucatan (Y), northern Atlantic lowlands (NAL), central highlands (CH), Costa Rica-western Panama (CRWP), eastern Panama-northern South America (EPNSA). Ancestral stands for the all-zero ancestor.

homoplasies, involving the presence of *C. cristatus* in the southern bloc and Yucatan and the absence of the ancestor of *C. cristatus* + *C. percarinatus* from central Mexico.

Discussion

Partitioned analyses

All putative synapomorphies of Tetrapoda and Amniota (Jamieson 1995a, 1999), Squamata (Jamieson 1995b) and Iguania (Vieira *et al.* 2004) are present in the sperm of coryto-phanids. Six sperm-derived characters are putative synapomorphies of Corytophanidae: a bilateral ridge in transverse sections of the acrosome complex (char. 1840), a fragmented epinuclear lucent zone (1844), a deep nuclear fossa (1847), the beginning of the fibrous sheath at ring structure 2 (1850), grossly enlarged fibres 3 and 8 in the midpiece (1851) and granulated dense bodies (1855). Nevertheless, we should be careful in interpreting these character states as synapomorphies because the sister taxon of Corytophanidae is unknown. Hence, what seems to be a synapomorphy (regarding the taxa and characters of the present work) could potentially become a reversal or convergence when more iguanian taxa are added. For example, a bilaterally ridged acrosome complex is present in the polychrotid *Anolis carolinensis* (Scheltinga *et al.* 2001), while granulated dense bodies are also present in the polychrotid *Polychrus acutirostris* (Teixeira *et al.* 1999a), in the crotaphytids *Crotaphytus bicinctores* and *Gambelia wislizenii* (Scheltinga *et al.* 2001). The chamaeleonid *Bradypodion karrooicum* also presents a deep nuclear fossa (Jamieson 1995b). However, the fragmented epinuclear lucent zone was never noticed before. This characteristic is apparently unique to Corytophanidae, since the sperm of almost all iguanian major lineages is currently described and none of them presents a similar structure. Hoplocercids (*Enyalioides laticeps* and *Hoplocercus spinosus*) and oplurids (*Oplurus cuvieri* and
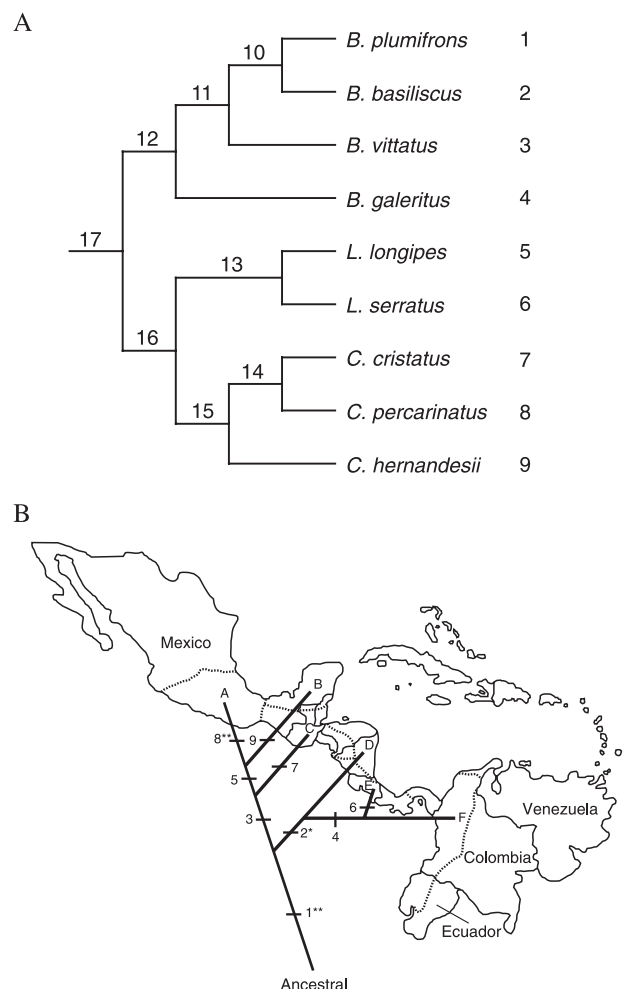
Fig. 5 A, B. —A. Phylogenetic relationships for species 1–9 used to construct the BPA data matrix. Each internal branch is numbered for matrix representation. —B. Area cladogram (19 steps, CI = 0.895, RI = 0.846) depicting the interrelationships among six Central American regions: A — central Mexico; B — Yucatan; C — central highlands; D — northern Atlantic lowlands; E — Costa Rica-western Panama; and F — eastern Panama-northern South America (see also Materials and Methods for further delimitation of each region). Asterisks show branches with homoplastic transformations. Internal branches are numbered to show the taxa supporting grouped areas: (1) *B. vittatus*, the ancestor of the group *B. basiliscus* + *B. plumifrons* + *Basiliscus vittatus*, the ancestor of *Basiliscus*, the ancestor of the group *C. cristatus* + *C. percarinatus**, the ancestor of *Corytophanes*, the ancestor of *Corytophanes* + *Laemanctus* and the ancestor of Corytophanidae; (2) *C. cristatus*** (dispersal) and *B. galeritus*; (3) *L. longipes*, *L. serratus* and the ancestor of *Laemanctus*; (4) *B. basiliscus* and the ancestor of the group *B. basiliscus* and *B. plumifrons*; (5) *C. hernadesii*; (6) *B. plumifrons*; (7) *C. percarinatus*; (8) the ancestor of *C. cristatus* + *C. percarinatus** (extinction); and (9) *C. cristatus***.

O. cyclurus), the only major iguanian lineages for which sperm morphology has never been described, also lack those structures (pers. obs.).

Since the first phylogenetic analyses of Squamata using sperm-derived data, both the number of species sampled and number of characters has increased considerably (Jamieson 1995b; Jamieson *et al.* 1996; Oliver *et al.* 1996; Teixeira *et al.* 1999a,b,c,d, 2002; Scheltinga *et al.* 2000, 2001; Giugliano *et al.* 2002; Tavares-Bastos *et al.* 2002; Teixeira 2003; Vieira *et al.* 2004). Nevertheless, sperm-derived data did not produce a completely resolved cladogram for iguanian lineages. Perhaps sperm-derived characters could be useful to clarify higher-level relationships, since they did not resolve the relationships within Corytophanidae. However, in terms of quality, these characters performed as well as morphological or molecular ones: nonparametric statistical comparisons of individual consistency indices (ci; excluding apomorphies) showed a significant difference among the three data partitions, with morphological characters having a significantly larger CI (as revealed by a Tukey test) than molecular characters (ANOVA on ranked CI: $F_{2,574} = 6.06$, $P = 0.0025$, $n = 577$; $CI_{(mol)} = 0.67 \pm 0.25$, $n = 486$; $CI_{(morph)} = 0.77 \pm 0.24$, $n = 66$; $CI_{(sperm)} = 0.74 \pm 0.19$, $n = 25$). Molecular data produced a fully resolved cladogram, but support for one group (*Corytophanes* + *Laemanctus*) was weak. In addition, morphological data did not produce a single cladogram and all of the four most parsimonious topologies recovered *Polychrus acutirostris* (Polychrotidae) as a member of Corytophanidae (although this relationship appears to be artificial, since it received low branch support). The more convincing hypothesis is that derived from the combined analysis of the three data partitions, highlighting the importance of using many classes of characters (e.g. behavioural, ecological, molecular, morphological and physiological) to access the historical relationships of a particular group.

Total evidence (combined) analysis
The combined analysis produces the best hypothesis for the historical relationships of corytophanid lizards. It was the only data set capable of recovering strongly supported clades (at least for Corytophanidae, its genera and for the relationship between *Corytophanes* and *Laemanctus*). Additionally, in view of the fact that there was no significant conflict among the data partitions (in the basis of support for their groups), we think each partition complements the other. Therefore, the proposal of Lang (1989), in which *Basiliscus* is the sister taxon of *Corytophanes* + *Laemanctus*, is corroborated by the present work, both by Bayesian and parsimony analyses. Lang (1989) also provided details concerning the systematics and vicariance/dispersal events for Corytophanidae.

Although Lang's hypothesis was not rejected, our parsimony analysis recovered clades not strongly supported in previous

works (relationships within *Basiliscus* and *Corytophanes*). This could result from missing data in our matrix, since missing data are frequently considered the most important impediment when data from diverse characters and taxa are combined (Wiens 2003). Curiously, this problem is not directly connected to the proportion of missing data and taxa with too few incomplete data are more prone to reduce phylogenetic accuracy (Wiens 2003). In this respect, our results seem to be paradoxical: the topology derived from the molecular partition (no missing data) is very similar to that derived from the combined analysis, with greater support for more inclusive nodes, but with weaker support for more exclusive nodes (e.g. *Corytophanes* plus *Laemanctus*). The combined-analysis topology (derived from a matrix with a larger amount of missing data) is the one with the greatest support for lower taxonomic ranks. This contradiction may be due to missing data, to heterogeneity in evolutionary rates among different data sets (Swofford 1991; Miyamoto & Fitch 1995), or a combination of both. Bayesian analysis shows strong support for the monophyly of *B. vittatus* plus *B. Basiliscus* and *B. plumifrons*.

In our view, only a more complete (or at least augmented) taxonomic sample for the data sets used here (and for any other kind of data) will corroborate or reject our hypothesis with a greater degree of reliability. This complete taxonomic sampling could also indicate whether the weakly supported groups are the results of rapid DNA evolution (leading to saturation in their sequences). Reduced intervals between speciation events could lead to a lack of support for the more exclusive taxa, since saturation reflects rapid DNA evolution. In this way, the lack of support for some more exclusive groups could be a true fact of the evolutionary history of Corytophanidae and not an artifactual result.

Brooks parsimony analysis
There exist three hypotheses for the origin of Corytophanidae (Lang 1989): North American, Central American and South American. Historically, the static continents of the north hemisphere were considered the main faunal stock from which some groups were transversally transmitted to the south (e.g. Matthew 1915; Schmidt 1943; Wiley 1981). However, there exists no compelling evidence for a North American origin of Corytophanidae, except for the thesis that the larger land masses of the north hemisphere were the main theatres of evolution and that its fauna and flora are superior and evolutionarily advanced relative to their southern hemisphere counterparts.

The presence of iguanian fossils from the Upper Cretaceous in South America and their absence from North America prior to the early Eocene (or middle Palaeocene) suggest a Gondwanan origin of the clade (Estes & Price 1973; Estes & Báez 1985; Albino 1996). Therefore, iguanians presumably entered North America in the Upper Cretaceous-early

Tertiary by waif dispersal across the more or less continuous Greater Antilles-Aves Ridge island arc (Gayet *et al.* 1992; Pitman *et al.* 1993) or, alternatively, through an interamerican dispersal corridor provided by the *in situ* formation of Central America (Briggs 1994). Stuart (1950) postulated that *Basiliscus* and *Laemanctus* evolved in Central America or on the Mexican Plateau from the prototypes of a faunal wave that entered Central America from the north, prior to the closure of the Eocene. Whether or not these early colonizers included the ancestral corytophanid is a matter of debate. For instance, Savage (1966, 1982) and Vanzolini & Heyer (1985) postulated that corytophanids are a Central American group that evolved north of the Panamanian portal, whereas Lang (1989: fig. 56) postulated a northward dispersal of the ancestral basiliscine (= corytophanid) stock from South America into Central America.

The BPA based on distributional and phylogenetic information of corytophanids suggests that the diversification of Corytophanidae took place in Central America and that the presence of the group in South America is relatively recent, thus favouring a Central American origin. Our analysis indicates a major division between northern and southern areas, the former being supported by the putative ancestor of *Laemanctus* and the latter by the presence of *Corytophanes cristatus* (likely by dispersal from northern areas) and *Basiliscus galeritus*. Further, the common ancestor of *Corytophanes* + *Laemanctus* and the common ancestor of *Basiliscus* were probably widespread in Central America, occurring in both groups of areas. Other biogeographicalal analyses of the Central American biota, including fishes (Murphy & Collier 1996), a combination of insect, fish, lizard and plant data (Marshall & Liebherr 2000), beetles (Morrone & Márquez 2001), plants (Ibarra-Manríquez *et al.* 2002) and mammals (Escalante *et al.* 2004), reached a similar conclusion, the differences between regions and geographicalal ranges among these studies notwithstanding.

Our northern clade roughly corresponds to the Sierra Transvolcanica, Sierra Madre del Sur and most of the Chiapan Guatemalan Highlands areas of endemism proposed by Marshall & Liebherr (2000), whereas our southern clade corresponds to their Talamancan Cordillera area of endemism. Likewise, using BPA those authors found a close relationship among the northern areas and postulated a major role of lowlands as geographical barriers. A latitudinal differentiation of the Central American biota is not surprising, considering the shape of the region and the fact that it lies between the Nearctic and Neotropical realms. Nevertheless, the boundary between the northern and southern groups of areas we uncovered does not correspond to the traditionally evoked Isthmus of Tehuantepec (Brown & Lomolino 1998), being apparently associated with the Nicaraguan lowlands. The emergence of highlands in southern Central America began approximately

3 Mya (Coates & Obando 1996), whereas the uplift of the Central American Plateau in northern Central America occurred between 10 and 3.8 Mya (Rogers *et al.* 2002), suggesting that the vicariance between the northern and southern areas is relatively recent. According to our area cladogram, this event is likely responsible for the divergence of *Laemanctus*.

In the northern clade, the Isthmus of Tehuantepec is apparently associated with the divergence between *Corytophanes hernandesii* and the common ancestor of *C. cristatus* and *C. percarinatus*, whereas the divergence between the two latter taxa is due to the rise of the Chiapas-Guatemalan highlands, home of *C. percarinatus*. In the southern clade, *Basiliscus galeritus* was the first taxon to diverge and to colonize northern South America, presumably after the closure of the Isthmus of Panama in the mid-Pliocene. A second colonization of northern South America, by *B. basiliscus*, occurred later. From late Miocene through early and perhaps middle Pleistocene, the Isthmus of Panama repeatedly alternated between a dry land bridge and a constricted waterway driven by the combination of active tectonics and oscillating sea-levels, associated with glacial (low sea-level) and interglacial (high sea-level) periods (Coates & Obando 1996; Beu 2001), promoting colonization and isolation, with subsequent differentiation of corytophanids in northern South America.

Conclusions

We conclude, in agreement with previous authors (Frost & Etheridge 1989; Lang 1989; Schulte *et al.* 2003), that Corytophanidae (*sensu* Frost & Etheridge 1989) is monophyletic, as indicated by Bayesian and parsimony analyses. Our analyses corroborate the hypothesis of Lang (1989) that *Basiliscus* is the sister taxon of *Corytophanes* plus *Laemanctus*. Furthermore, the monophyly of the three corytophanid genera is here corroborated. The BPA suggested a Central American origin of Corytophanidae and that Late Tertiary events, including epeirogenic uplifts and the formation on lowlands in Central America and the closure of the Panamanian portal, were the major source for vicariance/dispersal episodes promoting the differentiation of the group.

Acknowledgements

References

Albino, A. M. (1996). The South American fossil Squamata (Reptilia: Lepidosauria). *Münchner Geowissenschaftliche Abhandlungen. Reihe A. Geologie und Paläontologie*, *30*, 185–202.

Beu, A. G. (2001). Gradual Miocene to Pleistocene uplift of the Central American isthmus: Evidence from tropical American tonnoidean gastropods. *Journal of Paleontology*, *75*, 706–720.

Bremer, K. (1994). Branch support and tree stability. *Cladistics*, *10*, 295–304.

Briggs, J. C. (1994). The genesis of Central America: biology versus geophysics. *Global Ecology and Biogeography Letters*, *4*, 169–172.

Brooks, D. R. (2001). How to do BPA, really. *Journal of Biogeography*, *28*, 345–358.

Brown, J. H. & Lomolino, M. V. (1998). *Biogeography*, 2nd edn. Sunderland, MA: Sinauer Associates, Inc.

Camp, C. L. (1923). Classification of the lizards. *Bulletin of the American Museum of Natural History*, *48*, 289–481.

Coates, A. G. & Obando, J. A. (1996). The geological history of Central America. In J. B. C. Jackson, A. F. Budd & A. G. Coates (Eds) *Evolution and Environment in Tropical America* (pp. 21–56). Chicago: The University of Chicago Press.

Escalante, T., Rodríguez, G. & Morrone, J. J. (2004). The diversification of Nearctic mammals in the Mexican transition zone. *Biological Journal of the Linnean Society*, *83*, 327–339.

Estes, R. D. & Báez, A. M. (1985). Herpetofaunas of North and South America during the Late Cretaceous and Cenozoic: evidence for interchange? In F. G. Stehli & S. D. Webb (Eds) *The Great American Biotic Interchange* (pp. 139–197). New York: Plenum Press.

Estes, R. & Price, L. I. (1973). Iguanid lizard from the Upper Cretaceous of Brazil. *Science*, *180*, 748–751.

Etheridge, R. & de Queiroz, K. (1988). A phylogeny of Iguanidae. In R. Estes & G. Pregill (Eds) *Phylogenetic Relationships of the Lizard Families. Essays Commemorating Charles L. Camp* (pp. 283–368). Stanford, California: Stanford University Press.

Felsenstein, J. (1985). Confidence limits on phylogenies with a molecular clock. *Systematic Biology*, *34*, 152–161.

Frost, D. R. & Etheridge, R. (1989). A phylogenetic analysis and taxonomy of iguanian lizards (Reptilia: Squamata). *Miscellaneous Publications of the Museum of Natural History, University of Kansas*, *81*, 1–65.

Frost, D. R., Etheridge, R., Janies, D. & Titus, T. A. (2001). Total evidence, sequence alignment, evolution of polychrotid lizards and a reclassification of the Iguania (Squamata: Iguania). *American Museum Novitates*, *3343*, 1–38.

Gayet, M., Rage, J.-C., Sempere, T. & Gagnier, P.-Y. (1992). Modalités des échanges de vertébrés continentaux entre l'Amérique du Nord et l'Amérique du Sud au Crétacé supérieur et au Paléocene. *Bulletin de la Société Géologique de France*, *163*, 781–791.

Giugliano, L. G., Teixeira, R. D., Colli, G. R. & Báo, S. N. (2002). Ultrastructure of spermatozoa of the lizard *Ameiva ameiva*, with considerations on polymorphism within the family teiidae (Squamata). *Journal of Morphology*, *253*, 264–271.

Grant, T. & Kluge, A. G. (2003). Data exploration in phylogenetic inference: scientific, heuristic, or neither. *Cladistics*, *19*, 379–418.

Huelsenbeck, J. P. & Ronquist, F. (2001). MRBAYES: Bayesian inference of phylogeny. *Bioinformatics*, *17*, 754–755.

Ibarra-Manríquez, G., Villaseñor, J. L., Durán, R. & Meave, J. (2002). Biogeographicalal analysis of the tree flora of the Yucatan Peninsula. *Journal of Biogeography*, *29*, 17–29.

Jamieson, B. G. M. (1995a). Evolution of tetrapod spermatozoa with particular reference to amniotes. In B. G. M. Jamieson, J. Ausio & J. Justine (Eds) *Advances in Spermatozoal Phylogeny and Taxonomy* (pp. 343–358). Paris, France: Muséum National d'Histoire Naturelle.

Jamieson, B. G. M. (1995b). The ultrastructure of spermatozoa of the Squamata (Reptilia) with phylogenetic considerations. In B. G. M. Jamieson, J. Ausio & J. Justine (Eds) *Advances in Spermatozoal Phylogeny and Taxonomy* (pp. 359–383). Paris, France: Muséum National d'Histoire Naturelle.

Jamieson, B. G. M. (1999). Spermatozoal phylogeny of the vertebrata. In C. Gagnon (Ed.) *The Male Gamete: From Basic Science to Clinical Applications* (pp. 303–331). Vienna, Illinois: Cache River Press.

Jamieson, B. G. M., Oliver, S. C. & Scheltinga, D. M. (1996). The ultrastructure of spermatozoa of Squamata. I. Scincidae, Gekkonidae and Pygopodidae (Reptilia). *Acta Zoologica (Stockholm)*, *77*, 85–100.

Lang, M. A. (1989). Phylogenetic and biogeographical patterns of basiliscine iguanians (Reptilia: Squamata: 'Iguanidae'). *Bonner Zoologische Monographien*, *28*, 1–172.

Lee, M. S. Y. (1998). Convergent evolution and character correlation in burrowing reptiles: Towards a resolution of squamate relationships. *Biological Journal of the Linnean Society*, *65*, 369–453.

Lewis, P. O. (2001). A likelihood approach to estimating phylogeny from discrete morphological character data. *Systematic Biology*, *50*, 913–925.

Macey, J. R., Larson, A., Ananjeva, N. B. & Papenfuss, T. J. (1997). Evolutionary shifts in three major structural features of the mitochondrial genome among iguanian lizards. *Journal of Molecular Evolution*, *44*, 660–674.

Maddison, W. P. & Maddison, D. R. (2001). *MacClade: Analysis of Phylogeny and Character Evolution*. Sunderland, Massachusetts: Sinauer Associates, Inc.

Marshall, C. J. & Liebherr, J. K. (2000). Cladistic biogeography of the Mexican transition zone. *Journal of Biogeography*, *27*, 203–216.

Matthew, W. D. (1915). Climate and evolution. *Annals of the New York Academy of Sciences*, *24*, 171–318.

McCranie, J. R. & Köhler, G. (2004a). *Laemanctus longipes. Catalogue of American Amphibians and Reptiles*, *795*, 1–4.

McCranie, J. R. & Köhler, G. (2004b). *Laemanctus serratus. Catalogue of American Amphibians and Reptiles*, *796*, 1–5.

McCranie, J. R., Townsend, J. H. & Wilson, L. D. (2004). *Corytophanes hernandesii. Catalogue of American Amphibians and Reptiles*, *790*, 1–6.

Miyamoto, M. M. & Fitch, W. M. (1995). Testing species phylogenies and phylogenetic methods with congruence. *Systematic Biology*, *44*, 64–76.

Morrone, J. J. & Márquez, J. (2001). Halffter's Mexican transition zone, beetle generalized tracks and geographicalal homology. *Journal of Biogeography*, *28*, 635–650.

Murphy, W. J. & Collier, G. E. (1996). Phylogenetic relationships within the aplocheiloid fish genus *Rivulus* (Cyprinodontiformes, Rivulidae): implications for Caribbean and Central American biogeography. *Molecular Biology and Evolution*, *13*, 642–649.

Oliver, S. C., Jamieson, B. G. M. & Scheltinga, D. M. (1996). The ultrastructure of spermatozoa of Squamata. II. Agamidae, Varanidae, Colubridae, Elapidae and Boidae (Reptilia). *Herpetologica*, *52*, 216–241.

Pitman, W. C. III, Cande, S., LaBrecque, J. & Pindell, J. (1993). Fragmentation of Gondwana: the separation of Africa from South America. In P. Goldblatt (Ed.) *Biological Relationships Between Africa and South America* (pp. 15–34). New Haven, Connecticut: Yale University Press.

Posada, D. & Crandall, K. A. (1998). Modeltest: testing the model of DNA substitution. *Bioinformatics*, *14*, 817–818.

Pough, F. H., Andrews, R. M., Cadle, J. E., Crump, M. L., Savitzky, A. H. & Wells, K. D. (1998). *Herpetology*. Upper Saddle River, New Jersey: Prentice Hall.

Rogers, R. D., Karason, H. & van der Hilst, R. D. (2002). Epeirogenic uplift above a detached slab in northern Central America. *Geology*, *30*, 1031–1034.

Savage, J. M. (1966). The origins and history of the Central American herpetofauna. *Copeia*, *4*, 719–766.

Savage, J. M. (1982). The enigma of Central American herpetofauna: dispersal or vicariance? *Annals of the Missouri Botanical Garden*, *69*, 464–547.

Scheltinga, D. M., Jameison, B. G. M., Trauth, S. E. & McAllister, C. T. (2000). Morphology of the spermatozoa of the iguanian lizards *Uta stansburiana* and *Urosaurus ornatus* (Squamata, Phrynosomatidae). *Journal of Submicroscopic Cytology and Pathology*, *32*, 261–271.

Scheltinga, D. M., Jameison, B. G. M., Espinoza, R. E. & Orrel, K. S. (2001). Descriptions of the mature spermatozoa of the lizards *Crotaphytus bicinctores*, *Gambelia wislizenii* (Crotaphytidae) and *Anolis carolinensis* (Polychrotidae) (Reptilia, Squamata, Iguania). *Journal of Morphology*, *247*, 160–171.

Schmidt, K. P. (1943). Corollary and commentary for 'Climate and Evolution'. *American Midland Naturalist*, *30*, 241–253.

Schulte, J. A., II. Macey, J. R., Larson, A. & Papenfuss, T. J. (1998). Molecular test of phylogenetic taxonomies: a general procedure and example using four subfamilies of the lizard family iguanidae. *Molecular Phylogenetics and Evolution*, *10*, 367–376.

Schulte, J. A., II. Valladares, J. P. & Larson, A. (2003). Phylogenetic relationships within Iguanidae inferred using molecular and morphological data and a phylogenetic taxonomy of iguanian lizards. *Herpetologica*, *59*, 399–419.

Schwenk, K. (1994). Systematics and subjectivity: the phylogeny and classification of iguanian lizards revisited. *Herpetological Review*, *25*, 53–57.

Simmons, M. P. & Ochoterena, H. (2000). Gaps as characters in sequence-based phylogenetic analyses. *Systematic Biology*, *49*, 369–381.

Sokal, R. R. & Rohlf, F. J. (1981). Taxonomic congruence in the Leptopodomorpha re-examined. *Systematic Zoology*, *30*, 309–325.

Stuart, L. C. (1950). A geographical study of the herpetofauna of Alta Verapaz, Guatemala. *Contributions from the Laboratory of Vertebrate Biology*, *45*, 1–77.

Swofford, D. L. (1991). When are phylogeny estimates from molecular and morphological data sets incongruent? In M. M. Miyamoto & J. Cracraft (Eds) *Phylogenetic Analysis of DNA Sequences* (pp. 295–333). Oxford: Oxford University Press.

Swofford, D. L. (2002). PAUP*. *Phylogenetic Analysis Using Parsimony (*and Other Methods)*. Sunderland, Massachusetts: Sinauer Associates.

Tavares-Bastos, L., Teixeira, R. D., Colli, G. R. & Báo, S. N. (2002). Polymorphism in the sperm ultrastructure among four species of lizards in the genus *Tupinambis* (Squamata: Teiidae). *Acta Zoologica (Stockholm)*, *83*, 297–307.

Teixeira, R. D. (2003). Análise filogenética da família Teiidae (Squamata, Reptilia), a ultra-estrutura de espermatozóide e a sua utilidade filogenética. UnPublishers Doctorate Thesis, Universidade Estadual de Campinas, Campinas, São Paulo.

Teixeira, R. D., Colli, G. R. & Báo, S. N. (1999a). The ultrastructure of spermatozoa of the lizard *Polychrus acutirostris* (Squamata, Polychrotidae). *Journal of Submicroscopic Cytology and Pathology*, *31*, 387–395.

Teixeira, R. D., Colli, G. R. & Báo, S. N. (1999b). The ultrastructure of the spermatozoa of the lizard *Micrablepharus maximiliani* (Squamata, Gymnophthalmidae), with considerations on the use of sperm ultrastructure characters in phylogenetic reconstruction. *Acta Zoologica (Stockholm)*, *80*, 47–59.

Teixeira, R. D., Colli, G. R. & Báo, S. N. (1999c). The ultrastructure of the spermatozoa of the worm-lizard *Amphisbaena alba* (Squamata, Amphisbaenidae) and the phylogenetic relationships of amphisbaenians. *Canadian Journal of Zoology*, 77, 1254–1264.

Teixeira, R. D., Scheltinga, D. M., Trauth, S. E., Colli, G. R. & Báo, S. N. (2002). A comparative ultrastructural study of spermatozoa of the teiid lizards, *Cnemidophorus gularis gularis*, *Cnemidophorus ocellifer* and *Kentropyx altamazonica* (Reptilia, Squamata, Teiidae). *Tissue and Cell*, *34*, 135–142.

Teixeira, R. D., Vieira, G. H. C., Colli, G. R. & Báo, S. N. (1999d). Ultrastructural study of spermatozoa of the neotropical lizards, *Tropidurus semitaeniatus* and *Tropidurus torquatus* (Squamata, Tropiduridae). *Tissue and Cell*, *31*, 308–317.

Townsend, J. H., McCranie, J. R. & Wilson, L. D. (2004a). *Corytophanes cristatus*. *Catalogue of American Amphibians and Reptiles*, *789*, 1–6.

Townsend, J. H., McCranie, J. R. & Wilson, L. D. (2004b). *Corytophanes percarinatus*. *Catalogue of American Amphibians and Reptiles*, *791*, 1–3.

Uetz, P., Etzold, T. & Chenna, R. (1995). The EMBL Reptile Database. http://www.embl-heidelberg.de/~uetz/LivingReptiles.html.

Vanzolini, P. E. & Heyer, W. R. (1985). The american herpetofauna and the interchange. In F. G. Stehli & S. D. Webb (Eds) *The Great American Biotic Interchange* (pp. 475–487). New York: Plenum Press.

Vieira, G. H. C., Colli, G. R. & Báo, S. N. (2004). The ultrastructure of the spermatozoon of the lizard *Iguana iguana* (Reptilia, Squamata, Iguanidae) and the variability of sperm morphology among iguanian lizards. *Journal of Anatomy*, *204*, 451–464.

Wiens, J. J. (2001). Character analysis in morphological phylogenetics: problems and solutions. *Systematic Biology*, *50*, 689–699.

Wiens, J. J. (2003). Missing data, incomplete taxa and phylogenetic accuracy. *Systematic Biology*, *52*, 528.

Wiley, E. O. (1981). *Phylogenetics: The Theory and Practice of Phylogenetic Systematics*. New York: Wiley-Interscience.

Wilkinson, M. (1992). Ordered versus unordered characters. *Cladistics*, *8*, 375–385.

Zug, G. R., Vitt, L. J. & Caldwell, J. P. (2001). *Herpetology. An Introductory Biology of Amphibians and Reptiles*, 2nd edn. San Diego, CA: Academic Press.

Appendix 1

Morphological and sperm-derived characters used in the phylogenetic analyses. Boldened numbers and names correspond to the character positions in the matrix and the character name, respectively. Sperm-derived characters range from 1840 to 1871; morphological ones range from 1872 to 1960. The number following each morphological character refers to the original character number from which those characters were 'first' used: 1872–1910 taken from Frost & Etheridge (1989); 1911–1960 taken from Lang (1989). The consistency index for each character is shown in parentheses (subsequent to the character name), followed by ordination status (when ordered). We excluded the following original characters to avoid any character being represented twice in our matrix: chars. 12, 14, 17, 19, 31, 32 and 42 of Lang (1989) and chars. 16, 18, 20, 25 and 44 of Frost & Etheridge (1989). Because of no variation among outgroup and ingroup taxa, some characters (1–4, 6, 15, 17, 19, 26–28, 49–53, 58, 60, 61, 63, 66 and 67) of Frost & Etheridge (1989) were also excluded from the data matrix.

1839/GapPos 1288–1290 (1.000): (0) absent, (1) present.

1840/Acrosome complex, ridge (1.000): (0) absent, (1) unilateral, (2) bilateral.

1841/Acrosome complex, unilateral electron-lucent space (0.500): (0) absent, (1) present.

1842/Acrosome, radial aspect of subacrosomal cone in transverse section (0.500): (0) absent, (1) present.

1843/Acrosome complex, ridge at the epinuclear electron lucent zone level (or acrosome flattening) (1.000): (0) poorly developed, (1) well developed.

1844/Epinuclear lucent zone, aspect (1.000): (0) entire, (1) fragmented.

1845/Perforatorium, base plate (0.667): (0) absent, (1) knoblike, (2) stopperlike.

1846/Nucleus, lacunae (1.000): (0) absent, (1) present.

1847/Nuclear fossa (1.000): (0) shallow, (1) deep.

1848/Neck region, stratified laminar structure (1.000): (0) bilateral, (1) bilateral and well-developed.

1849/Neck region, electron-dense structure inside the proximal centriole (0.500): (0) absent, (1) present.

1850/Midpiece, beginning of the fibrous sheath in the midpiece (0.500): (0) not applicable, (1) level of mitochondria tier 1–2, (2) tier 2–3, (3) tier 3–4, (4) at ring structure 2, (5) at ring structure 3.

1851/Midpiece, fibres 3 & 8 (0.500): (0) grossly enlarged, (1) not grossly enlarged.

1852/Midpiece, number of sets of mitochondria and ring structures (0.667 ordered): (0) not applicable, (1) 3, (2) 4, (3) 5, (4) 6.

1853/Midpiece, mitochondria in oblique section (1.000): (0) columnar, (1) slightly curved, (2) rounded.

1854/Midpiece, mitochondrial shape in longitudinal section (1.000): (0) trapezoidal, (1) rounded ends, (2) totally round.

1855/Midpiece, dense bodies (0.500): (0) solid, (1) granulated.

1856/Midpiece, dense bodies forming ring structures (1.000): (0) not applicable, (1) absent, (2) present.

1857/Midpiece, appearance of dense bodies in the ring structures in oblique section (1.000): (0) not applicable, (1) fused, forming compact structures, (2) not fused.

1858/Principal piece, fibres 3 & 8 at the anteriormost region (1.000): (0) absent, (1) present.

1859/Head length (0.618): (0) 0, (1) 1, (2) 2, (3) 3, (4) 4, (5) 5, (6) 6.

1860/Midpiece length (0.730): (0) 0, (1) 1, (2) 2, (3) 3, (4) 4, (5) 5, (6) 6.

1861/Tail length (0.600): (0) 0, (1) 1, (2) 2, (3) 3, (4) 4, (5) 5, (6) 6.

1862/Total length (0.585): (0) 0, (1) 1, (2) 2, (3) 3, (4) 4, (5) 5, (6) 6.

1863/Acrossome length (0.796): (0) 0, (1) 1, (2) 2, (3) 3, (4) 4, (5) 5, (6) 6.

1864/Epinuclear lucent zone length (0.528): (0) 0, (1) 1, (2) 2, (3) 3, (4) 4, (5) 5, (6) 6.

1865/Epinuclear lucent zone width (0.806): (0) 0, (1) 1, (2) 2, (3) 3, (4) 4, (5) 5, (6) 6.

1866/Nuclear rostrum length (0.691): (0) 0, (1) 1, (2) 2, (3) 3, (4) 4, (5) 5, (6) 6.

1867/Nuclear shoulders width (0.828): (0) 0, (1) 1, (2) 2, (3) 3, (4) 4, (5) 5, (6) 6.

1868/Nuclear base width (0.666): (0) 0, (1) 1, (2) 2, (3) 3, (4) 4, (5) 5, (6) 6.

1869/Distal centriole length (0.814): (0) 0, (1) 1, (2) 2, (3) 3, (4) 4, (5) 5, (6) 6.

1870/Nuclear length (0.538): (0) 0, (1) 1, (2) 2, (3) 3, (4) 4, (5) 5, (6) 6.

1871/Percentage of fibrous sheath occupancy into the midpiece (0.748): (0) 0, (1) 1, (2) 2, (3) 3, (4) 4, (5) 5, (6) 6.

1872/Lacrimal (5) (1.000): (0) present, (1) absent.

1873/Skull rugosity (7) (0.500): (0) absent or restricted to frontal bone, (1) extensive.

1874/Jugal, squamosal contact (8) (1.000): (0) not or barely in contact, (1) broadly juxtaposed.

1875/Postfrontal (9) (0.500): (0) present, (1) extremely small or absent.

1876/Parietal roof shape (10) (1.000): (0) trapezoidal, (1) V or Y-shaped, (2) Y-shaped with posteriorly directed median crest developed postembryonically, (3) Y-shaped with median crest developed embrionically.

1877/Parietal foramen (11) (1.000): (0) at frontoparietal suture or in parietal, (1) entirely within the frontal.

1878/Supratemporal (12) (1.000; ordered): (0) mostly on the lateral or ventral surface of the supratemporal process of

the parietal, (1) mostly on the medial surface of the supratemporal process of the parietal, (2) mostly in a groove in the ventral margin supratemporal process of the parietal.

1879/Osseous labyrinth (13) (0.500): (0) low to moderate elevation of the osseous labyrinth above the general level of the opisthotics, (1) high elevation above the general level of opisthotics.

1880/Endolymphatic sacs (14) (1.000): (0) do not extend outside of otic capsule into nuchal musculature, (1) extend in nuchal musculature.

1881/Splenial, anterior extent (21) (0.667; ordered): (0) extends anteriorly to or beyond 1/2 length of tooth row, (1) does not extend anteriorly more than 1/2 length of tooth row, (2) does not extend anteriorly more than 1/6 length of tooth row.

1882/Splenial, posterior extent (22) (0.500): (0) terminates posteriorly anterior to anterior edge of mandibular fossa, (1) terminates posterior to, or at anterior edge of mandibular fossa.

1883/Angular, condition of contact with splenial (23) (1.000): (0) angular large; suture with splenial on lingual face, (1) angular small. Suture with splenial on ventral or labial face.

1884/Posterior mylohyoid foramen (24) (0.667; ordered): (0) anterior to or approximately at the level of superior apex of coronoid, (1) between level of superior apex of coronoid and anterior end of adductor fossa, (2) posterior to anterior end of adductor fossa.

1885/Ceratobranchials (29) (1.000): (0) second not reaching clavicles, (1) reaching the clavicles.

1886/Clavicle (30) (1.000): (0) flat, with wide lateral flange, (1) flange small or absent.

1887/Insertion of clavicle (31) (0.500): (0) on suprascapula, (1) on scapula.

1888/Interclavicle (32) (1.000): (0) anterior process absent, (1) anterior process well developed.

1889/Sternum, anterior extent (33) (0.500): (0) sternum does not approach junction of posterior and lateral processes of interclavicle closely, (1) sternum approaches junction of posterior and lateral processes of interclavicle closely.

1890/Caudal vertebral type (34) (1.000): (0) *Sceloporus* condition, (1) *Iguana* condition, (2) *Basiliscus* condition (3) anole condition.

1891/Scapular fenestra (35) (1.000): (0) present, (1) absent.

1892/Posterior coracoid fenestra (36) (0.500): (0) present (1) absent.

1893/Median enlarged sternal fontanelle(s) (37) (1.000; ordered): (0) absent or small, often hiden by interclavicle, (1) present, large and not paired, (2) present, large and paired.

1894/Cervical ribs (38) (0.500; ordered): (0) first pair on vertebra number 3, (1) on number 4, (2) on number 5.

1895/Number of sternal ribs (39) (0.667; ordered): (0) 4, (1) 3, (2) 2 or fewer.

1896/Postxiphisternal inscriptional ribs (40) (1.000; ordered): (0) all attached proximally to dorsal ribs and none are confluent midventrally, (1) one or more pairs attached to dorsal ribs and are confluent midventrally, (2) none attached to dorsal ribs or continuous midventrally.

1897/Tail autotomy fracture planes (41) (0.500): (0) present, (1) absent.

1898/Interparietal scale (42) (1.000): (0) small or absent, (1) large, as wide as interorbital space.

1899/Subocular scale (45) (0.500): (0) at least one scale below the eye conspicuously enlarged, (1) scales below the eye subequal.

1900/Mid-dorsal scale row (46) (1.000): (0) present, (1) absent.

1901/Gular fold (47) (0.500): (0) complete medially, (1) incomplete or absent.

1902/Femoral pores (48) (0.500): (0) present, (1) absent.

1903/Nasal chamber, S-condition (54) (1.000): (0) primitive condition, (1) S-condition, septomaxilla ploughshare shaped.

1904/Nasal chamber, fusion of nasal concha to roof of nasal chamber (55) (1.000): (0) primitive condition, (1) fusion of concha to roof of nasal chamber.

1905/Nasal chamber, anole condition (56) (1.000): (0) primitive condition, (1) nasal concha lost.

1906/Dorsal shank muscle innervation (59) (0.500): (0) A-condition (peroneus), (1) B-condition (interosseus).

1907/Hemipenis, capitation and sulci (61) (1.000; ordered): (0) unicapitate or weakly bilobate without distinctly divided sulci, (1) bilobate with distinctly divided sulci, (2) strongly bicapitate.

1908/Hemipenis, m/retractor lateralis posterior (62) (1.000): (0) not substantially situated within the hemipenial sheath, (1) substantially situated within the hemipenial sheath.

1909/Hemipenis, dorsal accessory sheath (64) (1.000): (0) absent, (1) present.

1910/Colic septa (65) (0.333): (0) absent, (1) present.

1911/Roof of nasal chamber (1) (1.000): (0) nasal capsule entirely covered by frontal and nasals, (1) nasal capsule uncovered at junction of frontal and nasals.

1912/Septomaxillae (2) (0.500; ordered): (0) present, contacting each other at midline, the maxillae anteriorly and lying on the top of the vomers, (1) present as small slivers of bone lying within the nasal cavity that do not contact each other at midline, (2) absent.

1913/Nasal median contact (3) (1.000; ordered): (0) separated by less than 50% of their length, (1) separated for more than 50% of their length by nasal process of premaxilla, (2) completely separated.

1914/Posterior margin of nasals (4) (0.667): (0) posterior aspect of nasals form a smooth curve, with apex in the middle of the bone, (1) posterior aspect of nasals pointed, (2) posterior aspect of nasals squared.

1915/Prefrontal-nasal relationship (5) (1.000; ordered): (0) broad contact between prefrontals and nasals, (1) small area of contact between prefrontals and nasals, with nasals separated anteriorly from prefrontals by prefrontal process of maxilla, (2) prefrontals completely separated from nasals by prefrontal process of maxilla and anterolateral process of frontal bone.

1916/Anterolateral spine of prefrontal (6) (1.000): (0) absent, (1) present, projecting anteriorly over the premaxillary process of maxilla.

1917/Groove at prefrontal-lacrimal junction (7) (0.500): (0) absent, (1) present.

1918/Palatine-ectopterygoid relationship (8) (1.000): (0) no contact between ectopterygoids and palatines, (1) ectopterygoids contact palatines; excluding maxillae from infraorbital foramen.

1919/Palatine process of pterygoid (9) (1.000): (0) does not project past the anteriormost border of infraorbital foramen, (1) extends anteriorly beyond the infraorbital foramen.

1920/Quadrate process of pterygoid (10) (0.500): (0) tapering posteriorly, of with parallel ventral and dorsal edges, but not expanded, (1) quadrate process of pterygoid expanded terminally.

1921/Shape of mid-sagittal section of frontal (11) (1.000): (0) anterior and posterior aspects of frontal bone curve ventrally, (1) frontal bone is flat in mid-sagittal section view, or anterior and posterior aspects of frontal bones curve dorsally.

1922/Squamosal process of julgal (13) (1.000): (0) thin squamosal process, (1) broad squamosal process.

1923/Posterior angle of jugal (15) (1.000): (0) not expanded posteroventrally, rounded, (1) expanded posteroventrally, with posteroventral aspect of jugal approaching the posterodorsal aspect.

1924/Supraorbital process (16) (1.000): (0) absent; postorbital and prefrontals lack processes, (1) intermediate condition; prefrontals have posteriorly directed process and postorbital have anteriorly directed processes, (2) postorbitals in contact with prefrontals via a supraorbital arch.

1925/Lateral shelves of adductor crest (18) (1.000; ordered): (0) absent or when present is small and restricted to the anterolateral aspect of the adductor ridge, (1) present along the lateral aspect of the parietal crest, (2) large, expanded laterally to partially overlie the supratemporal opening.

1926/Development of the parietal blade (20) (1.000): (0) postembryonic development of median parietal blade, (1) embryonic development of parietal blade.

1927/Parietal blade sexual dimorphism (21) (1.000): (0) parietal blade well-developed in males only, (1) parietal blade well-developed in both sexes.

1928/Expansion of parietal blade (22) (1.000): (0) absence of parietal blade, (1) dorsal expansion, (2) ventral expansion.

1929/Dorsal process of squamosal (23) (0.500): (0) prominent dorsal 'hook' contacting the supratemporal, (1) no dorsal 'hook', i.e. ventral projection equals dorsal projection.

1930/Squamosal (24) (0.500): (0) curves dorsally, not contacting or overlapping the anterodorsal aspect of the quadrate (single articulation), (1) straight, overlapping the anterodorsal border of lateral concha of quadrate, with sharp laterally pointed spine (double articulation).

1931/Medial concha of quadrate (25) (0.500): (0) expanded medially past the cephalic condyle; the medial concha may or may not contact the anterolateral process of the paraoccipital process, (1) not expanded past the condyles (constricted).

1932/Quadrate (26) (1.000): (0) posterior crest arches anteriorly, (1) posterior crest is vertical with no anterior curvature.

1933/Epipterygoids (27) (1.000): (0) contacting the ventral portion of parietal, (1) free or contacting the alar process of prootic.

1934/Crista ventrolateralis (28) (1.000): (0) broad, expanded laterally obscuring the vidian canal, (1) narrow, not expanded laterally.

1935/Outlines of bony labyrinth (29) (0.667; ordered): (0) superficial outlines of bony labyrinth obscure, not raised above the surface of the occiptal bones, (1) intermediate condition, (2) superficial outlines of bony labyrinth very distinct, raised well above the surface of the occipital bones.

1936/Posttemporal fenestra (30) (1.000; ordered): (0) open, with the squamosal process at an angle of more than 90 degrees, (1) partially closed, (2) closed, owing to the limiting angle of the squamosal process of parietal (less than 90 degrees).

1937/Coronoid lateral process (33) (0.500; ordered): (0) coronoid bone with a small, irregular process overlapping the posterolateral surface of dentary, (1) a posteriorly directed curving process descends over the posterodorsal surface of the dentary, (2) coronoid bone without a process overlapping the posterolateral surface of the dentary.

1938/Size of posterior aspect of angular (labial view) (34) (0.500): (0) extends between coronoid process and articular fossa, (1) lateral aspect reduced, does not extend between the coronoid process and the articular fossa.

1939/Angular process size (35) (1.000): (0) well defined in juveniles and adults (nontransforming ontogeny), (1) small in juveniles and well-defined only in large specimens.

1940/Angular process position (36) (1.000): (0) angular process positioned in a horizontal plane, (1) positioned in a oblique plane.

1941/Hyoid apparatus pattern (37) (0.333): (0) z-pattern in wich the second ceratobranchial is the shortest posterior element, the first ceratobranchial and the ceratohyal being of equal length, (1) x-pattern; the second ceratobranchial is the longest element, the first ceratobranchial and the ceratohyal may or may not be equal in length.

1942/Rostral position of skull (38) (0.500): (0) arched dorsally, (1) rostral position of skull is pointed or keel-shaped (spatulate).

1943/Crowns of posterior marginal teeth (39) (0.500): (0) tricuspid, with more or less paralell sides, (1) tricuspid, with distinctly expanded crowns, (2) tricuspid, with distinctly tapered crowns and very small secondary cusps.

1944/Number of presacral vertebrae (40) (uninformative): (0) 24, (1) 23, (2) 22.

1945/Lumbar ribs (41) (1.000): (0) all with free articulating ribs, (1) one or more with ribs absent.

1946/Ratio of number of neural spines to number of transverse process in caudal vertebrae (43) (1.000): (0) 1/1 ratio, (1) 2/1 ratio.

1947/Neural spine height (44) (0.667 ordered): (0) neural spines same size as vertebral body, (1) neural spines enlarged in thoracic, lumbar and caudal regions in males, (2) neural spines reduced, shorter than height of vertebral body.

1948/Rib articulation patterns (45) (0.750): (0) 6(4 + 2), (1) 7(4 + 3), (2) 5(3 + 2), (3) 6(3 + 3).

1949/Suprascapular cartilages (46) (1.000): (0) project dorsally to the level of the vertebrae, sometimes meet above neural spines, (1) suprascapular cartilages do not reach the level of the vertebral column.

1950/Dorsal extent of clavicle (47) (0.500): (0) clavicle reaches the suprascapular cartilages, with the acromion process located on suprascapular cartilage or at the scapulo-suprascapular junction, (1) clavicle does not reach the suprascapular cartilages, with acromion process located on anterior aspect of scapula.

1951/Clavicular lateral margin (48) (0.500): (0) lateral margin of clavicle irregular, or forming a smooth curve, (1) lateral margin of clavicle distinctly angular, with an acute projection at the apex of the angle.

1952/Clavicular fenestrae (49) (0.500): (0) absent, (1) present.

1953/Preacetabular process (50) (1.000): (0) prominent, (1) reduced.

1954/Anterior extension of symphysis pubis (51) (1.000): (0) symphysis pubis does not extend anteriorly past the pubic tubercles, (1) symphysis pubis extends anteriorly past the pubic tubercles with pubic rami join together forming an acute angle.

1955/Infratemporal fascia (52) (1.000): (0) fascia present, variably covering the posterodorsal aspect of the infratemporal fossa to the entire M/adductor mandibulae externus, (1) little fascia present at posterodorsal corner of infratemporal fossa.

1956/Insertion of M. adductor mandibulae externus (53) (0.333): (0) mandibular insertion projects past the surangular, (1) mandibular insertion restricted to surangular.

1957/M. levator anguli oris (54) (1.000): (0) origin includes the tympanic crest of the quadrate, (1) does not originate from the tympanic crets of the quadrate.

1958/M. adductor mandibulae externus superficialis (55) (1.000): (0) single dorsal head, (1) two separate dorsal heads.

1959/M. adductor mandibulae externus profundus (56) (1.000; ordered): (0) dorsal head well developed, (1) dorsal head reduced, (2) dorsal head is absent.

1960/Superciliary scales (57) (0.500; ordered): (0) elongate and strongly overlapping, (1) intermediate, (2) quadrangular, nonoverlapping.

Appendix 2

List of apomorphies for the clades of Corytophanidae. The state for each character is given for each clade and is followed by the character number, the character transformation and by the status of the character change in each node or branch (ACCTRAN optimization), respectively, in parenthesis. When a morphometric character transformation is given, then its cost (length) is also presented inside the parenthesis. Apomorphies for Corytophanidae (predominantly) must be interpreted with caution, because no all nine iguanian major lineages are represented in this analysis (see Discussion).

Corytophanidae (*sensu* Frost & Etheridge 1989): a bilateral ridge in transverse sections of the acrosome complex (char. 1840; 1→2; unambiguous); a fragmented epinuclear lucent zone (char. 1844; 0→1; unambiguous); a deep nuclear fossa (char. 1847; 0→1; unambiguous); beginning of the fibrous sheath at ring structure 2 (char. 1850; 2→4; ambiguous); grossly enlarged fibres 3 and 8 in the midpiece (char. 1851; 1→0; unambiguous); granulated dense bodies (char. 1855; 0→1; unambiguous); epinuclear lucent zone length (char. 1864; 1→4; ambiguous; (408); epinuclear lucent zone width (char. 1865; 1→6; unambiguous; (271); nuclear shoulders width (char. 1867; 2→6; unambiguous; (405); nuclear base width (char. 1868; 2→4; ambiguous; (81); distal centriole length (char. 1869; 2→4; unambiguous; (13); percentage of fibrous sheath occupancy into the midpiece (char. 1871; 1→6; ambiguous; (129); a extremely small or absent postfrontal (char. 1875; 0→1; ambiguous); a 'Y-shaped with posteriorly directed median crest developed postembryonically' parietal roof shape (char. 1876; 1→2; ambiguous); a V- or Y-shaped parietal foramen (char. 1877; 0→1; unambiguous); the splenial extends anteriorly to or beyond 1/2 length of tooth row (char. 1881; 1→0; ambiguous); *Basiliscus* condition of the caudal vertebral (char. 1890; 1→2; ambiguous); scapular fenestra present (char. 1891; 0→1; unambiguous); posterior

coracoid fenestra present (char. 1892; 0→1; ambiguous); a B-condition (interosseus) of the dorsal shank muscle innervation (char. 1906; 0→1; unambiguous); m. retractor lateralis posterior of hemipenis substantially situated within the hemipenial sheath (char. 1908; 0→1; unambiguous); groove at prefrontal-lacrimal junction present (char. 1917; 0→1; ambiguous); quadrate process of pterygoid expanded terminally (char. 1920; 0→1; ambiguous); dorsal expansion of parietal blade (char. 1928; 0→1; ambiguous); a posteriorly directed curving process descends over the posterodorsal surface of the dentary in the coronoid lateral process (char. 1937; 2→1; ambiguous); clavicular fenestrae present (char. 1952; 0→1; ambiguous); mandibular insertion of m. adductor mandibulae externus projects past the surangular (char. 1956; 1→0; ambiguous); additionally, more 50 unambiguous and 54 ambiguous molecular char. transformations are present in this node.

Basiliscus: electron-dense structure inside the proximal centriole absent (char. 1849; 1→0; ambiguous); midpiece length (char. 1860; 5→4; ambiguous; (90); acrosome length (char. 1863; 6→4; ambiguous; (30); epinuclear lucent zone width (char. 1865; 6→4; ambiguous; (127); nuclear rostrum length (char. 1866; 6→4; ambiguous; (43); nuclear shoulders width (char. 1867; 6→4; ambiguous; (379); at least one sub-ocular scale below the eye conspicuously enlarged (char. 1899; 1→0; unambiguous); a 'broad, expanded laterally obscuring the vidian canal' crista ventrolateralis (char. 1934; 0→1; unambiguous); coronoid bone with a small, irregular process overlapping the posterolateral surface of dentary (char. 1937; 1→0; unambiguous); angular process positioned in a horizontal plane (char. 1940; 1→0; unambiguous); 1 : 1 ratio of number of neural spines to number of transverse process in caudal vertebrae (char. 1946; 0→1; unambiguous); symphysis pubis extends anteriorly past the pubic tubercles with pubic rami join together forming an acute angle (char. 1954; 0→1; unambiguous); additionally, more 13 unambiguous and 25 ambiguous molecular char. transformations are present in this node.

Basiliscus vittatus + (Basiliscus basiliscus + Basiliscus plumifrons): no morphological or sperm-derived characters are assigned to this node. Thirty-six unambiguous and 17 ambiguous molecular character transformations are present in this node.

Basiliscus basiliscus + Basiliscus plumifrons: neural spines enlarged in thoracic, lumbar and caudal regions of males (char. 1947; 0→1; unambiguous); Eighty-eight ambiguous molecular character transformations are assigned to this node.

Basiliscus plumifrons: colic septa present (char. 1910; 0→1; unambiguous); hyoid apparatus with x-pattern.

Basiliscus vittatus: Eighty-nine unambiguous and 19 ambiguous molecular character transformations are assigned to this branch.

Basiliscus galeritus: colic septa present (char. 1910; 0→1; unambiguous); further 62 unambiguous and 15 ambiguous molecular character transformations are present in this branch.

Basiliscus basiliscus: no character transformations could be assigned to this branch.

Corytophanes + Laemanctus: head length (char. 1859; 4→5; ambiguous; (44); tail length (char. 1861; 4→6; unambiguous; (207); total length (char. 1862; 4→6; unambiguous; (224); distal centriole length (char. 1869; 4→5; unambiguous; (7); jugal and squamosal broadly juxtaposed (char. 1874; 0→1; unambiguous); a 'Y-shaped with posteriorly directed median crest developed embryonically' parietal roof shape (char. 1876; 2→3; ambiguous); tail autotomy fracture planes absent (char. 1897; 0→1; unambiguous); septomaxillae present as small slivers of bone lying within the nasal cavity that do not contact each other at midline absent (char. 1912; 0→1; ambiguous); frontal bone is flat in mid-sagittal section view, or anterior and posterior aspects of frontal bones curve dorsally (char. 1921; 0→1; unambiguous); posterior angle of julgal expanded posteroventrally, with posteroventral aspect of jugal approaching the posterodorsal aspect (char. 1923; 0→1; unambiguous); lateral shelves of adductor crest present along the lateral aspect of the parietal crest (char. 1925; 0→1; unambiguous); embryonic development of parietal blade (char. 1926; 0→1; unambiguous); parietal blade well-developed in both sexes (char. 1927; 0→1; unambiguous); ventral expansion of parietal blade (char. 1928; 1→2; ambiguous); no dorsal 'hook' (i.e. ventral projection equals dorsal projection) in squamosal (char. 1929; 0→1; ambiguous); medial concha of quadrate not expanded, past the condyles (constricted) (char. 1931; 0→1; unambiguous); posterior crest of quadrate is vertical with no anterior curvature (char. 1932; 0→1; unambiguous); superficial outlines of bony labyrinth very distinct, raised well above the surface of the occipital bones (char. 1935; 1→2; unambiguous); angular process small in juveniles and well-defined only in large specimens (char. 1939; 0→1; unambiguous); rostral position of skull is pointed or keel-shaped (spatulate) (char. 1942; 0→1; unambiguous); crowns of posterior marginal teeth tricuspid, with more or less paralell sides (char. 1943; 1→0; unambiguous); one or more lumbar ribs with ribs absent (char. 1945; 0→1; unambiguous); prominent paracetabular process (char. 1953; 1→0; unambiguous); 'dorsal head reduced' state of m. adductor mandibulae externus profundus (char. 1959; 0→1; unambiguous); intermediate state of superciliary scales (char. 1960; 0→1; ambiguous); additionally, more 16 unambiguous and 21 ambiguous molecular char. transformations are assigned to this node.

Laemanctus: tail length (char. 1861; 6→5; ambiguous; (80); total length (char. 1862; 6→5; ambiguous; (59); acrosome length (char. 1863; 6→5; ambiguous; (82); epinuclear lucent zone length (char. 1864; 4→5; ambiguous; (131); epinuclear lucent zone width (char. 1865; 6→5; ambiguous; (241); nuclear rostrum length (char. 1866; 6→5; ambiguous; (176); nuclear shoulder width (char. 1867; 6→5; ambiguous; (24); nuclear base width (char. 1868; 4→5; ambiguous; (217);

nuclear length (char. 1870; 4→5; ambiguous; (168); percentage of fibrous sheath occupancy within the midpiece (char. 1871; 4→5; ambiguous; (5); extensive skull rugosity (char. 1873; 0→1; unambiguous); postfrontal present (char. 1875; 1→0; ambiguous); neural spines reduced, shorter than height of vertebral body (char. 1947; 0→2; unambiguous); 7(4+3) rib articulation pattern (char. 1948; 0→1; ambiguous); little fascia present at posterodorsal corner of infratemporal fossa (char. 1955; 0→1; unambiguous); 'two separate dorsal heads' aspect of m. adductor mandibulae externus superficialis (char. 1958; 0→1; unambiguous); quadrangular, nonoverlapping superciliary scales (char. 1960; 1→2; unambiguous); more 116 molecular char. transformations are assigned to this node.

Laemanctus serratus: posterior aspect of nasals squared (char. 1914; 0→2; unambiguous); 6(3 + 3) rib articulation pattern (char. 1948; 1→3; ambiguous).

Laemanctus longipes: no character transformations could be assigned to this branch.

Corytophanes: head length (char. 1859; 5→6; ambiguous; (45); epinuclear lucent zone length (char. 1864; 4→6; ambiguous; (355); nuclear base width (char. 1868; 4→5; ambiguous; (8); distal centriole length (char. 1869; 5→6; ambiguous; (110); nuclear length (char. 1870; 4→6; ambiguous; (8); percentage of fibrous sheath occupancy into the midpiece (char. 1871; 4→6; ambiguous; (202); osseous labyrinth with high elevation above the general level of opisthotics midpiece (char. 1879; 0→1; unambiguous); (char. 1879; 0→1; unambiguous); splenial does not extend anteriorly more than 1/2 length of tooth row (char. 1881; 0→1; ambiguous); insertion of clavicle on scapula (char. 1887; 0→1; unambiguous); nasal capsule uncovered at junction of frontal and nasals (char. 1911; 0→1; unambiguous); nasal median contact separated for more than 50% of their length by nasal process of premaxilla (char. 1913; 0→1; unambiguous); posterior aspect of nasals pointed (char. 1914; 0→1; unambiguous); small area of contact between prefrontals and nasals, with nasals separated anteriorly from prefrontals by prefrontal process of maxilla (char. 1915; 0→1; unambiguous); anterolateral spine of prefrontal present, projecting anteriorly over the premaxillary process of maxilla (char. 1916; 0→1; unambiguous); groove at prefrontal-lacrimal junction absent (char. 1917; 1→0; ambiguous); palatine process of pterygoid extends anteriorly beyond the infraorbital foramen (char. 1919; 0→1; unambiguous); quadrate process of pterygoid tapering posteriorly, of with parallel ventral and dorsal edges, but not expanded (char. 1920; 1→0; ambiguous); broad squamosal process (char. 1922; 0→1; unambiguous); supraorbital process with intermediate condition: prefrontals have posteriorly directed process and postorbital have anteriorly directed processes (char. 1924; 0→1; ambiguous); lateral shelves of adductor crest large, expanded laterally to partially overlie the

supratemporal opening (char. 1925; 1→2; unambiguous); squamosal straight, overlapping the anterodorsal border of lateral concha of quadrate, with sharp laterally pointed spine (double articulation) (char. 1930; 0→1; ambiguous); epipterygoids free or contacting the alar process of prootic (char. 1933; 0→1; unambiguous); post-temporal fenestra partially closed (char. 1936; 0→1; unambiguous); posterior aspect of angular (labial view) with lateral aspect reduced, does not extend between the coronoid process and the articular fossa (char. 1938; 0→1; unambiguous); lateral margin of clavicle distinctly angular, with an acute projection at the apex of the angle (char. 1951; 0→1; unambiguous); clavicular fenestrae absent (char. 1952; 1→0; ambiguous); mandibular insertion of of m. adductor mandibulae externus restricted to surangular (char. 1956; 0→1; ambiguous); m. levator anguli oris does not originate from the tympanic crest of the quadrate (char. 1957; 0→1; unambiguous); dorsal head of m. adductor mandibulae externus profundus absent (char. 1959; 1→2; unambiguous); more 80 ambiguous molecular character transformations are asserted to this node.

Corytophanes cristatus + Corytophanes percarinatus: postorbitals in contact with prefrontals via a supraorbital arch in the supraorbital process (char. 1924; 1→2; ambiguous); post-temporal fenestrae closed, owing to the limiting angle of the squamosal process of parietal (less than 90 degrees) (char. 1936; 1→2; unambiguous); coronoid bone with a small, irregular process overlapping the posterolateral surface of dentary (char. 1937; 1→0; unambiguous); x-pattern of hyoid apparatus present (char. 1941; 0→1; unambiguous); clavicle does not reach the suprascapular cartilages, with acromion process located on anterior aspect of scapula (char. 1950; 0→1; unambiguous).

Corytophanes cristatus: nasal median contact completely separated by nasal process of premaxilla (char. 1913; 1→2; unambiguous); prefrontals completely separated from nasals by prefrontal process of maxilla and anterolateral process of frontal bone (char. 1915; 1→2; unambiguous); ectopterygoids contact palatines, excluding maxillae from infraorbital foramen (char. 1918; 0→1; unambiguous); squamosal curves dorsally, not contacting or overlapping the anterodorsal aspect of the quadrate (single articulation) (char. 1930; 1→0; ambiguous); suprascapular cartilages do not reach the level of the vertebral column (char. 1949; 0→1; unambiguous); 56 unambiguous and 19 ambiguous molecular character transformations are also assigned to this branch in addition.

Corytophanes percarinatus: 43 unambiguous and 14 ambiguous molecular character transformations are assigned to this branch.

Corytophanes hernandesii: splenial terminates posterior to, or at anterior edge of, mandibular fossa (char. 1882; 0→1; unambiguous); 5(3 + 2) rib articulation pattern (char. 1948; 0→2; unambiguous).